frontiers | Frontiers in Earth Science

TYPE Original Research
PUBLISHED 19 August 2022
DOI 10.3389/feart.2022.935508

OPEN ACCESS

EDITED BY
Shuai Yin,
Xi'an Shiyou University, China

REVIEWED BY
Xinghua Wang,
SINOPEC Petroleum Exploration and Production Research Institute, China
Yaxiong Sun,
SINOPEC Petroleum Exploration and Production Research Institute, China

*CORRESPONDENCE
Xuanlong Shan,
shanxl@jlu.edu.cn

SPECIALTY SECTION
This article was submitted to Structural Geology and Tectonics, a section of the journal Frontiers in Earth Science

RECEIVED 04 May 2022
ACCEPTED 19 July 2022
PUBLISHED 19 August 2022

CITATION
Wang W, Yi J, Shan X, Zhang X, Liu X, Liu P and Ren S (2022), Characteristics of fractures development and its controlling factors within the buried hill reservoirs from the Archaean metamorphic basement in the Bozhong Sag, Bohai Bay Basin, Eastern China. *Front. Earth Sci.* 10:935508. doi: 10.3389/feart.2022.935508

Characteristics of fractures development and its controlling factors within the buried hill reservoirs from the Archaean metamorphic basement in the Bozhong Sag, Bohai Bay Basin, Eastern China

Wei Wang[1], Jian Yi[1], Xuanlong Shan[1]*, Xintao Zhang[2], Xiaojian Liu[2], Pengcheng Liu[1] and Shuyue Ren[1]

[1]College of Earth Sciences, Jilin University, Changchun, China, [2]Tianjin Branch of China National Offshore Oil Corporation Ltd., Tianjin, China

Metamorphic rocks have almost no primary pore space, and their formation of large-scale reservoirs depends on fractures and related secondary pore space formed by tectonic and fluid activities. The BZ19-6 block in the Bozhong Sag, Bohai Bay Basin, is the largest and deepest buried basement condensate field of buried-hill in the world, and its reservoirs are characterized by strong heterogeneity. In this paper, we systematically summarize the characteristics of fracture development, explore the main factors controlling fracture development, establish a fracture development model and clarify the influence of fractures on reservoir quality by using core and microscopic thin section observations, physical property data, imaging logging data and 3D seismic data analysis. The results show that the major types of fractures in the study area are tectonic fractures and dissolution fractures. In particular, the tectonic fractures are widely developed, accounting for 71.7% of the total number of fractures. Migmatization controls the lithological distribution of Archean metamorphic rocks. The migmatitic granite, having the highest degree of migmatization, is the dominant lithology for fracture development because it is rich in brittle minerals, such as feldspar and quartz. Strong compressional orogeny occurred during Indosinian period when many fractures initially developed, which become dominant among the tectonic fractures. Compression-tension-compression multistage tectonic movements characterized the Yanshanian period. During this period, fractures of different degrees formed. The Himalayan period, critical for fracture reconstruction, reactivated the early fractures and promoted the positive influence of atmospheric freshwater and organic acids on fracture reconstruction. Fractures are distributed unevenly in the vertical direction, and fracture-intensive zones are the main development sites for favourable reservoirs because they enhance the porosity and permeability of Archean metamorphic rocks. It means that these fractures can provide effective storage

space for oil and gas, which is key for the formation of large-scale reservoirs. In addition, fractures can provide migration channels for organic acids and atmospheric freshwater, which lead to later dissolution, and connect various dispersed dissolution pores to improve the effectiveness of reservoir space.

KEYWORDS

Archean metamorphic rocks, buried hill, fracture characteristics, controlling factor, metamorphic reservoir, Bohai Bay basin

1 Introduction

With the continuous vertical development of oil and gas exploration, basement buried hills have become increasingly important targets in the exploration of hydrocarbon-bearing basins (Hou et al., 2019). To date, several medium to large oil and gas fields in buried hills of metamorphic rocks have been discovered worldwide, such as the Bach Ho oil field in the Cuu Long Basin, Vietnam (Cuong and Warren, 2009); the La Paz-Mara gas field in Venezuela (Nelson et al., 2000); the Aryskum oil and gas field in the South Turgay Basin, Kazakhstan (Han et al., 2020); the buried hill in the Bongor Basin, Chad (Dou et al., 2015; Li et al., 2017); and the Xinglongtai buried hill in the Liaohe Depression, China (Song et al., 2011). The Bohai Bay Basin is an important hydrocarbon-bearing basin in China, and important achievements and breakthroughs have been made in the exploration of buried hills of metamorphic rocks for oil and gas in the past 50 years, including the discovery of JZ25-1S, CFD18-1/2, BZ26-2, BZ19-6, BZ13-2, JZ25-3 and other oil and gas fields (Li et al., 2012; Zhao et al., 2015; Ye et al., 2021b). In particular, the discovery of the BZ19-6 gas field, which is the largest and deepest buried basement condensate field of buried hill in the world, shows the great exploration potential of deep buried hill of metamorphic rocks in the Bohai Bay Basin (Xie et al., 2018).

Buried hills of metamorphic rock have unique characteristics, such as a weak influence of burial depth, large reservoir thickness and strong physical heterogeneity (Luo et al., 2005; Liu et al., 2020). Metamorphic rocks have almost no primary pore space (Ni et al., 2011, 2013), and the formation of large-scale reservoirs in such rocks depends on fractures and related secondary pore space formed by tectonic activity, so fractures play an important role in reservoirs (Ameen et al., 2010; Carvalho et al., 2013; Guo et al., 2017; Hou et al., 2019). A large number of drilling records have shown that there are abundant hydrocarbons within the fractures in the Archean buried hills of metamorphic rocks in the Bohai Bay Basin (Yang et al., 2016; Xue and Li, 2018), indicating that fractures not only are effective pathways for hydrocarbon migration and enhance the permeability of reservoirs (Carvalho et al., 2013; Liu et al., 2016; Ye et al., 2020b), but also serve as the main storage space for the accumulation of hydrocarbons (Luo et al., 2005; Parnell, 2010; Ding et al., 2013; Shen et al., 2015; Guo et al., 2016). Hence, for dense metamorphic rocks, the degree of fracture development determines the scale and production of reservoirs (Tong et al., 2012).

At present, many scholars have carried out studies on fractures in buried hills of metamorphic rocks (Fu et al., 2003; Eig and Bergh, 2011; Zou et al., 2013; Achtziger-Zupančič et al., 2017; Li et al., 2020; Ye et al., 2021b). It is believed that the distribution and development of fractures are controlled by lithology, strata thickness, weathering intensity, stress and other factors (Bazalgette et al., 2010; Zeng et al., 2013; Wang et al., 2016; Yin et al., 2019; Chen et al., 2021; Zhao et al., 2021). Under the same tectonic stress conditions, rocks rich in brittle minerals, such as felsic minerals, are more likely to produce fractures (Ye et al., 2021b). Weathering and eluviation can cause irregular fractures of different scales to form near the surface of rocks, resulting in a high degree of rupture and well-developed fractures (Salah and Alsharhan, 1998; Yue et al., 2014). Tectonics is a key factor contributing to fracture generation in rocks. The intensity of active faults is strongly correlated with fracture density (Maerten et al., 2018). In addition, faults control the development of fractures by affecting the local tectonic stress around them, and the closer fractures are to faults, the more intense the fractures are (Ye et al., 2021a). In the vertical direction, folds can be divided from top to bottom into tensile strain zones, transition zones and shortening zones according to stress changes. In the tensile strain zone, tensile fractures develop, while shear fractures develop in the shortening zone (Li et al., 2018).

Some scholars have studied the fractures of buried hills of metamorphic rocks in the Bohai Bay Basin (Tong et al., 2012; Ye et al., 2020b), and they have mostly focused on reservoir descriptions, identifying tectonic fractures and dissolution fractures as the main reservoir spaces (Zhou et al., 2005; Hou et al., 2019). However, no clear fracture development model is available that can comprehensively illustrate the development of fractures and accurately predict buried hills of metamorphic rocks reservoirs. To address this limitation, taking the Bozhong Sag in the Bohai Sea area as an example, we integrate core and microscopic thin section observations, physical property data, imaging logging data and 3D seismic data analysis to systematically summarize the characteristics of fracture development, explore the main controlling factors of fracture development, and establish a fracture development model to clarify the impact of fractures on reservoir quality. These research results are of great importance to fracture prediction and the effective development of buried hill in the study area, and provide insight that can guide the future exploration of buried hill reservoirs.

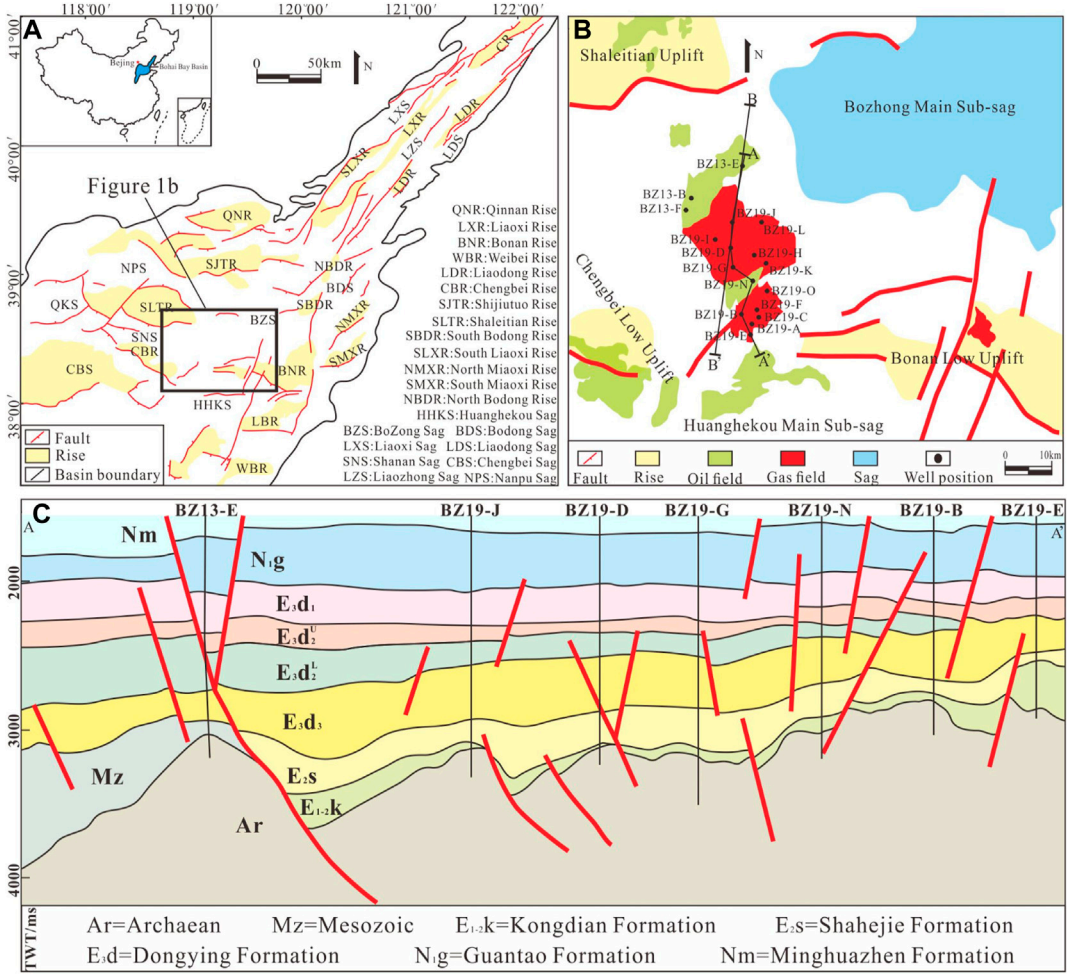

FIGURE 1
Geological features of the Bohai Bay Basin. **(A)** Location of the study area in the Bohai Bay Basin (modified after Ye et al., 2020); **(B)** Simplified structural map of the Bozhong Sag (modified after Xue & Li, 2018); **(C)** Typical geological section through BZ19-6 and adjacent areas (location of the section see Figure 1B)).

2 Geological setting

The Bohai Bay Basin with an area of 20×10^4 km^2, in eastern China, is a Mesozoic and Cenozoic superimposed basin developed on the base of the Paleozoic craton in North China via strike-slip and pull-apart interactions (Allen et al., 1997; Hou et al., 2001; Li et al., 2010; Liang et al., 2016). The Bozhong Sag, a secondary tectonic unit, is the largest hydrocarbon-generating sag in the Bohai Bay Basin (Wan et al., 2009). It is surrounded by the Jiao-Liao uplift to the east, Chengning uplift to the west, Liaodong Bay Depression to the north and Jiyang Depression to the south and has an area of approximately 2×10^4 km^2 (Figure 1A) (Xu et al., 2019). Since the Mesozoic, the Bozhong Sag has experienced a series of intense tectonic movements, forming a complex fracture system mainly composed of normal faults and locally developed strike-slip faults (Li et al., 2010). These faults control not only the structural evolution of the basin but also the formation and distribution of the basement hydrocarbon reservoir (Tong et al., 2015).

The tectonic evolution of the basin created favourable geological conditions for the formation of buried hills in basement uplifts. During this evolution, the Luliang movement involved strong migmatization and granitization, and the Jining, Galidon and Haixi tectonic movements were the main orogenic movements during the Paleozoic era; these movements manifested as vertical uplift in the North China Platform, resulting in the absence of Upper Ordovician-lower Carboniferous sedimentation (Qi et al., 2013). During the Indosinian period, due to the collision between the South China and North China plates (Wang et al., 2018), the Bozhong Sag was subjected to a nearly S-N oriented

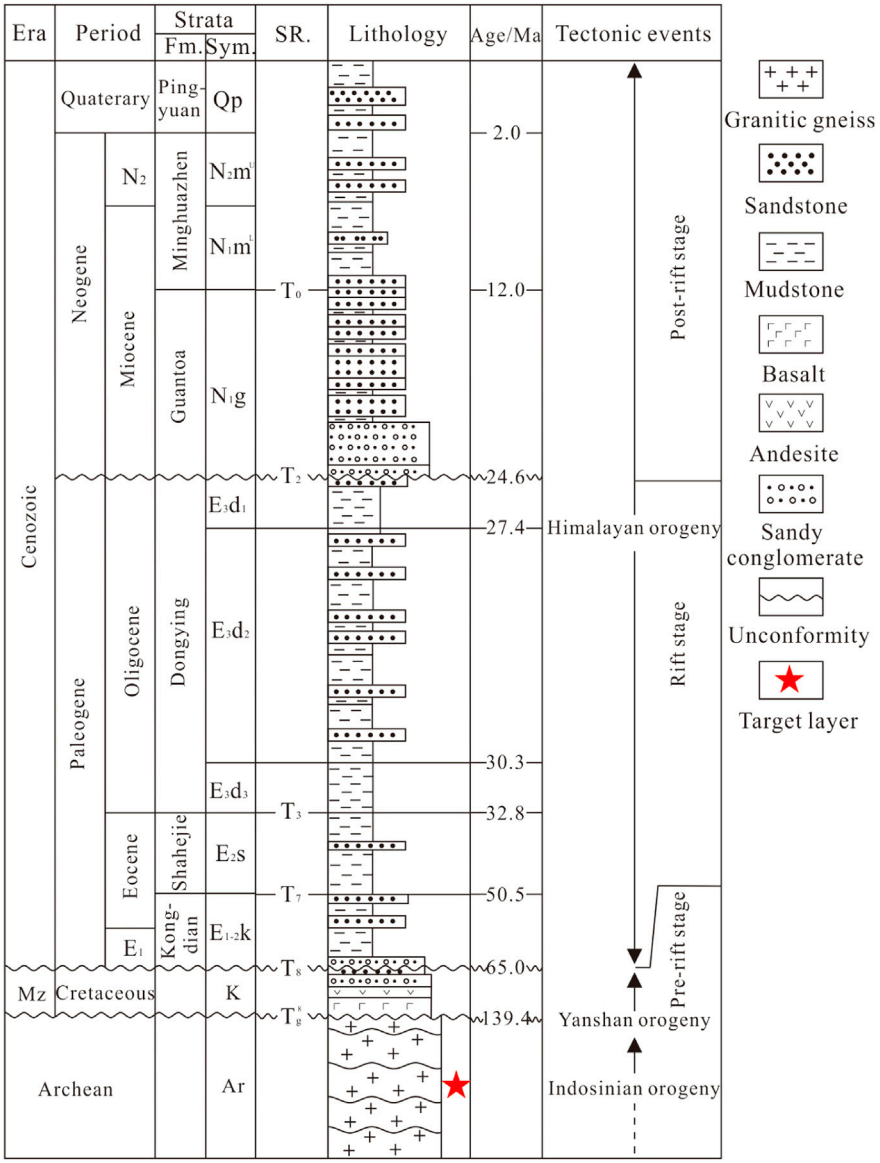

FIGURE 2
Stratigraphic column in the study area, showing the lithology and tectonic event (modified after Zhao et al., 2020). Fm.=Formation; Sym.=Submember; SR.=Seismic reference; Mz=Mesozoic; E_1=Paleocene; N_2=Pliocene.

compressional stress field, which produced a series of folds nappe from south to north and nearly W-E oriented thrust fault systems (Li et al., 2013; Wang et al., 2019b, 2019a), resulting in an E-W oriented uplift-sag pattern. At this time, tectonic movement played a crucial role in the formation of buried hills (Yu and Koyi, 2016). Under the influence of NE-oriented subduction and the retreat of the Paleo-Pacific plate during the Yanshanian period (Hou et al., 1998), the basin experienced three stages of tectonic evolution, namely, early Yanshanian compression-torsion, middle Yanshanian tension and late Yanshanian compression-torsion (Zhou et al., 2003), and developed a series of NE-oriented faults and associated fold structures (Wang et al., 2019b; 2019a); these tectonic activities caused widespread deformation in the North China Craton region and was the key period of buried hills deformation (Figure 1C) (Li et al., 2013; Zhu et al., 2017). The Himalayan period was mainly influenced by the India-Eurasia plate collision and the subduction of the Pacific plate; the pre-existing NE-oriented and nearly W-E oriented large-scale faults were reactivated (Qi et al., 2013; Peng et al., 2018; Wang et al., 2018), and a series of alternating topographic depressions and uplifts formed between the fault zones.

The study area is located on the deep structural ridge in the southwestern part of the Bozhong Sag in the Bohai Bay Basin. It is adjacent to the Bonan low uplift in the southeast and is connected to the Chengbei low uplift in the southwest, Huanghekou Sag in the south and Bozhong Sag in the north. This area shows the characteristics of an uplifted anticline structural belt (Hou et al., 2019) (Figure 1B). Drilling wells in the study area encountered, from top to bottom, the Quaternary Pingyuan Formation (Qp), Neogene Minghuazhen Formation ($N_{2\text{-}1}M$) and Guantao Formation (N_2g); Paleogene Dongying Formation (E_3d), Shahejie Formation ($E_{3\text{-}2}S$), and Kongdian Formation ($E_{2\text{-}1}K$); and Mesozoic (Mz) and Archean (Ar) strata. Mesozoic, Paleozoic and Proterozoic strata are completely absent in the BZ19-6 block. The Archean buried hill in the BZ13-2 block is partially covered by Mesozoic rocks. Archean metamorphic rocks compose the oldest crystalline basement in the Bozhong Sag and are the main object of this study. The burial depth is approximately 4000–5500 m (Figure 2), and it is the deepest buried hill reservoir of metamorphic rock in the Bohai Bay Basin.

3 Data and methods

We identified the lithologies and fracture types by observing eight wells (BZ19-B, BZ19-G, BZ19-J, BZ19-K, BZ19-L, BZ19-N, BZ19-O, BZ13-E) with a total core length of 51.7 m and 306 sidewall cores and determined the development of fractures and the degree of filling. A total of 277 ordinary and casting thin sections were collected and observed to identify the microscopic characteristics of features, filling and dissolution along microfractures. Casting thin sections (30 μm thick) with blue dye resin and cathodoluminescence were used to analyse the effective cracks and pores (Nabway and Kassab, 2013; Lai et al., 2019). The clay minerals and microstructure were observed by scanning electron microscopy (SEM). A total of 136 analyses of reservoir physical property, including porosity and permeability, and 13 analyses of whole-rock diffraction were collected to obtain the mineral composition of different rock types.

Logging data, including conventional and imaging logging data from 18 wells, were obtained to interpret the fracture characteristics, including orientation, dip angle, scale, and fracture density (Cui et al., 2013). In this study, we calculated the fracture linear density as the total number of fractures per unit core length or the total number of fractures divided by the total length in the imaging log data (Ortega et al., 2006). In particular, the linear density discussed in this paper is the uncorrected original density. The principle of fracture occurrence identification by imaging logging is as follows: For any plane that is not parallel or perpendicular to the well axis and intersects with the drilling hole, its intersection surface is an elliptical surface, which is displayed as a sine wave curve on the expanded diagram (Li et al., 2020). The core observation is a statistical calculation of all fractures visible to eyes, including short fractures with small openings that cannot be detected by imaging logs and fractures parallel to the well axis. Therefore, the fracture linear density calculated by imaging logging is much lower than that observed in cores due to the different observation scales and methods of core and imaging logging. In addition, a 3D seismic dataset of approximately 1824 km^2 covering the study area was obtained from the Tianjin Branch of the China National Offshore Oil Corporation. The size of each data bin was 25 m × 25 m, and the overall vertical sampling rate of the seismic volume was 2 ms with a primary frequency of 35 Hz. All the above information was provided by the Tianjin Branch of China National Offshore Oil Corporation.

4 Results

4.1 Lithological characteristics

The lithologies of the Archean buried hills in the study area are mainly regional metamorphic rocks formed from Archean (tonalite-trondhjemite-granodiorite; TTG) protoliths under different degrees of migmatization (Zhang et al., 2019; Ye et al., 2021a), which can be further divided into migmatitic granite (Figures 3A,B), migmatitic gneiss (Figures 3C,D) and gneiss (Figures 3E,F) according to migmatization degree. The migmatitic granite is light in overall colour with granitic metamorphic structure, and the few melanosomes are usually distributed with veins as sparse streaks and spots (Figure 3A). These rocks are mainly composed of quartz, plagioclase and alkali feldspar (Figure 3B), of which felsic light-coloured minerals account for a large proportion, with contents of 80–90%, and only a small amount of biotite is present (<5%) (Table 1). The melanosome content is higher in the migmatitic gneiss, which is usually distributed in massive and strips in the groundmass (Figure 3C). In thin sections under crossed-polarized light, the feldspar surfaces appear strongly altered, and a small amount of biotite is weakly curved (Figure 3D). X-ray diffraction (XRD) data show that the felsic content is reduced to 60–80%, and the contents of biotite and hornblende are increased compared with those of migmatitic granite, accounting for 10–20% of the total (Table 1). After partial melting of the original rock occurs during migmatization, the felsic component is separated, and the remainder is rich in dark minerals, which together form gneiss (Vanderhaeghe et al., 1999). The degree of migmatization is lowest in the gneiss, and the columnar minerals are oriented, with an obvious gneissic structure (Figures 3E,F). The gneiss is mainly composed of plagioclase, quartz and biotite. The XRD data show that the biotite content of these rocks reaches 30% (Table 1). Most of the biotite is lamellar and elongated with bending deformation characteristics and strong chloritization, and it shows weak banding and schistosity (Figure 3F). In addition to the regional metamorphic rocks, some intrusive rocks (mainly diabase) are

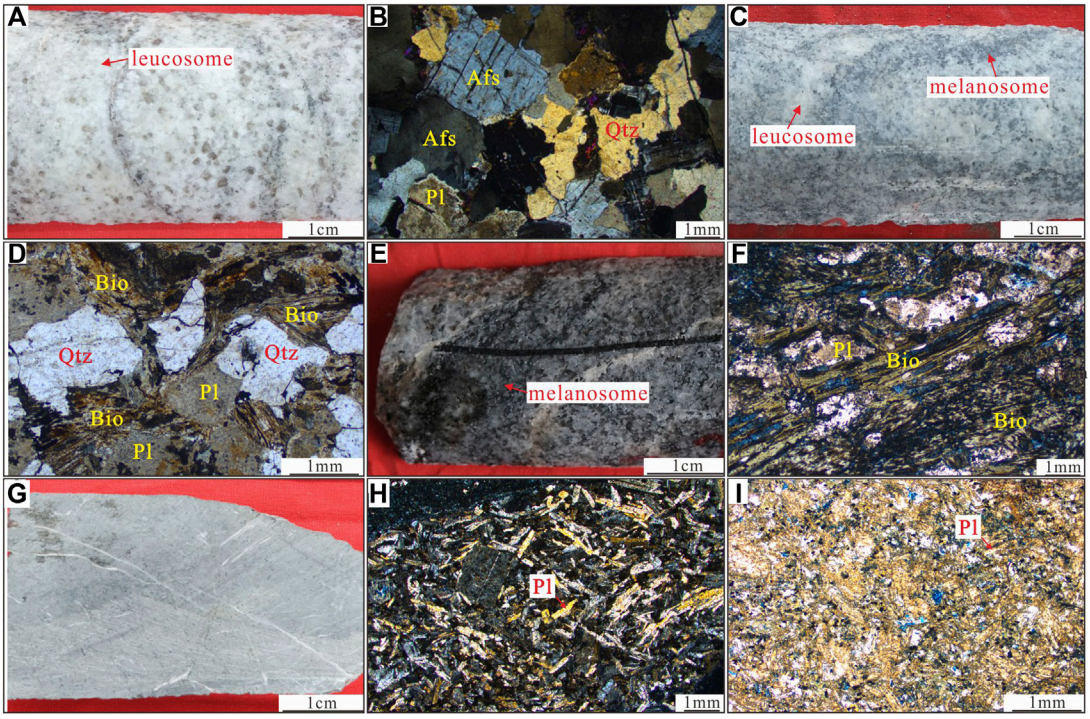

FIGURE 3
Petrological characteristics of the Archean metamorphic rocks in the study area. **(A)** Migmatitic granite, core, with a typical granitic metamorphic structure and many leucosomes, BZ13-E, 4718m; **(B)** Migmatitic granite, thin section, with plagioclase, K-feldspar and quartz, BZ19-G,4597m; **(C)** Migmatitic gneiss, core, the melanosome are usually distributed in massive and strips in the matrix, BZ13-E, 4717m; **(D)** Migmatitic gneiss, thin section, the feldspar surface is strongly altered, BZ19-N, 4490m; **(E)** gneiss, core, with obvious gneissic structure, BZ19-K, 5127m; **(F)** gneiss, thin section, most biotite is lamellar and shows strong chloritization, BZ19-G, 4613m; **(G)** diabase, core, BZ19-O, 4867m; **(H)** diabase, thin section, with a typical gabbroic structure, BZ19-B, 4076m; **(I)** diabase, thin section, with intense alteration, BZ19-G, 4830m; Qtz=quartz, Pl = plagioclase, Afs = alkaline feldspar, Bio=biotite.)

TABLE 1 X-ray diffraction (XRD) analyses showing the whole-rock mineralogy of intrusions and metamorphic rocks from the Bozhong sag (weight Percent, %).

Well	Depth/m	Qtz	Kfs	Pl	Cal	Dol	Py	Ank	Hbl	Cl	Bi	Lithology
BZ19-6-I	4955	24.0	31.0	33.0	3.0	-	-	-	-	4.0	5.0	Migmatitic Granite
BZ19-6-I	5305	22.0	22.0	39.0	6.0	1.0	-	-	-	4.0	6.0	
BZ19-6-K	5126	26.0	9.0	56.0	-	-	-	2.0	-	3.0	4.0	
BZ19-6-K	5127	27.0	17.0	47.0	-	-	-	3.0	-	2.0	4.0	
BZ19-6-K	4800	18.2	8.0	36.1	4.8	-	0.3	-	9.0	12.6	11.0	Migmatitic Gneiss
BZ19-6-M	4682	12.5	6.6	50.1	4.6	1.0	0.4	-	3.0	6.1	15.7	
BZ19-6-M	4602	17.3	6.9	46.5	8.1	-	-	-	-	7.0	14.2	
BZ19-6-M	4882	18.0	11.7	36.4	2.6	1.7	2.7	-	5.0	8.0	13.9	
BZ19-6-K	5127	23.0	10.0	31.0	1.0	-	-	1.0	-	3.0	31.0	Gneiss
BZ19-6-M	4560	18.5	7.7	32.3	6.1	-	2.2	-	3.2	4.0	26.0	
BZ19-6-O	5310	12.0	16.7	30.2	3.5	-	-	-	-	7.8	29.8	
BZ19-6-O	4868	17.6	12.0	36.2	0.8	-	1.6	0.3	-	30.2	1.3	Diabase
BZ19-6-I	5250	23.1	8.4	27.1	13.8	-	-	-	1.5	22.3	3.8	

Qtz=quartz, Kfs=K-feldspar, Pl=plagioclase, Cal=calcite, Dol=dolomite, Py=pyrite, Ank=ankerite, Hbl= hornblende, Cl= clay, Bi=biotite.

TABLE 2 Main fracture types of Archaean metamorphic rocks in the study area.

Types	Subtypes	Charateristics	Formation mechanism
Tectonic fractures	Tension fracture	They have unstable occurrence, short lengths, and rough surfaces and are surrounded by mineral grains. Unfilled or half-filled fractures are usually predominant	When the local extensional tectonic stress exceeds the ultimate tensile strength of the rock itself, the rock fracture produces tension fractures
	Shear fracture	They occur consistently, are straight and smooth, and cut mineral grains; they often appear as conjugate X shapes. Shear fractures are commonly filled with ankerite and calcite	When the three principal stresses are compressive stresses and the derived shear stress exceeds the limit of the shear strength of the rock itself, a shear fracture is generated
	Micro fracture	In feldspar, they usually form along the cleavage planes and appear as regular and straight cracks; in quartz, they usually appear as disordered cracks	Microfractures are fractures less than 100 mm with width and less than 10 mm in length, and their genesis is the same as that of macro fractures. Microfractures are often developed at the defects or weak points of rocks, such as the cleavage planes of minerals and the boundaries of mineral grains
Dissolution fractures	Weathering dissolution fracture	They usually have a rough surface, network distribution, irregular shape and high density. They are interlaced and connected with dissolution pores and fractures and are often found on the tops of buried hill	On the basis of the original fractures, weathering and dissolution reconstruction in the later period are superimposed
	Inner dissolution fracture	The core is "dendritic" and the fracture wall is irregular and not smooth; they are mostly developed near faults	Under the influence of deep fluid or organic acid, the original rock minerals or cement in the buried hills are dissolved into fractures, which make the original fractures expand and extend

scattered in the buried hills within the study area. The diabase has a typical gabbroic structure (Figure 3G). The main phenocrysts are plagioclase (Figure 3H). The mafic intrusions tend to show intense alteration (Figure 3I), with clay mineral contents reaching 20% (Table 1). The Archean buried hills have undergone multistage fluid alteration and multistage filling in pores and fractures. The XRD and thin sections show that the filling materials mainly include ankerite, calcite and clay minerals.

4.2 Fracture development characteristics

After the formation of the Archean metamorphic basement in the Bohai Bay Basin, a large number of fractures developed through long-term complex tectonic movements. We call these fractures related to tectonic activity tectonic fractures (Aydin, 2000), those related to mineral dissolution are called dissolution fractures (Liu et al., 2020). According to their formation mechanisms, scale and formation positions, tectonic fractures can be subdivided into tension fractures, shear fractures and microfractures (Zhao et al., 2020), and dissolution fractures can be subdivided into weathering and inner dissolution fractures. Through detailed observations and descriptions, and consideration of with the regional geological setting, the main fracture types and characteristics are identified and summarized (Table 2; Figure 4).

4.2.1 Tectonic fractures

The tectonic fractures are unevenly distributed through the cores (Figure 4). Tension fractures are generally caused by ruptures in the direction perpendicular to the inferred stress when the extensional tectonic stress exceeds the tensile strength of the rock itself (Wang et al., 2017). These fractures appear to be unstable in occurrence, short, and quite wide, with rough surfaces in the core, as shown by the surrounding minerals (Figure 4A). Tension fractures are usually poorly filled (Figure 4A). Shear fractures are formed when the rock is ruptured by applying shear force that exceeds the rock shear strength (Lyu et al., 2017; Zhang et al., 2020). Core observations reveal that the planar morphology is generally conjugate X-shaped; shear fractures commonly develop in groups and are characterized by stable occurrence, a straight and smooth appearance, and small crack openings (Figure 4A). This morphology is also seen in the penetration of cut mineral grains (Wang et al., 2017). Shear fractures are commonly filled with ankerite and calcite (Figure 4A).

Microfractures are very common in these metamorphic rocks according to thin section observations and SEM (Figure 4E-O), with widths less than 0.5 mm. According to the relationship between fractures and mineral particles, three types of microfractures have been identified: 1) intra-particle fractures, 2) inter-particle fractures and 3) trans-particle fractures. Inter-particle fractures mainly occur between mineral grains, and their length is limited by the grain edges. They are commonly widely developed within alkaline feldspar (mainly micro plagioclase) and quartz. In feldspars, the intra-particle fractures are usually ruptured along with cleavage fractures. They have regular and straight features (Figure 4E), with a width of 6 μm (Figure 4N). However, in quartz, the intra-particle fractures usually appear as disordered cracks (Figure 4F). Microcracks with a width of 4 μm are visible under scanning electron microscope (Figure 4O). Inter-particle fractures are developed on the edges of mineral grains, which shows the phenomenon of surrounding mineral grains (Figure 4G). Trans-particle fractures cut through the mineral grains, and the cut mineral grains are often relatively displaced, with regular and straight shapes and long extents (Figures 4H–J). The trans-particle fractures directly displace

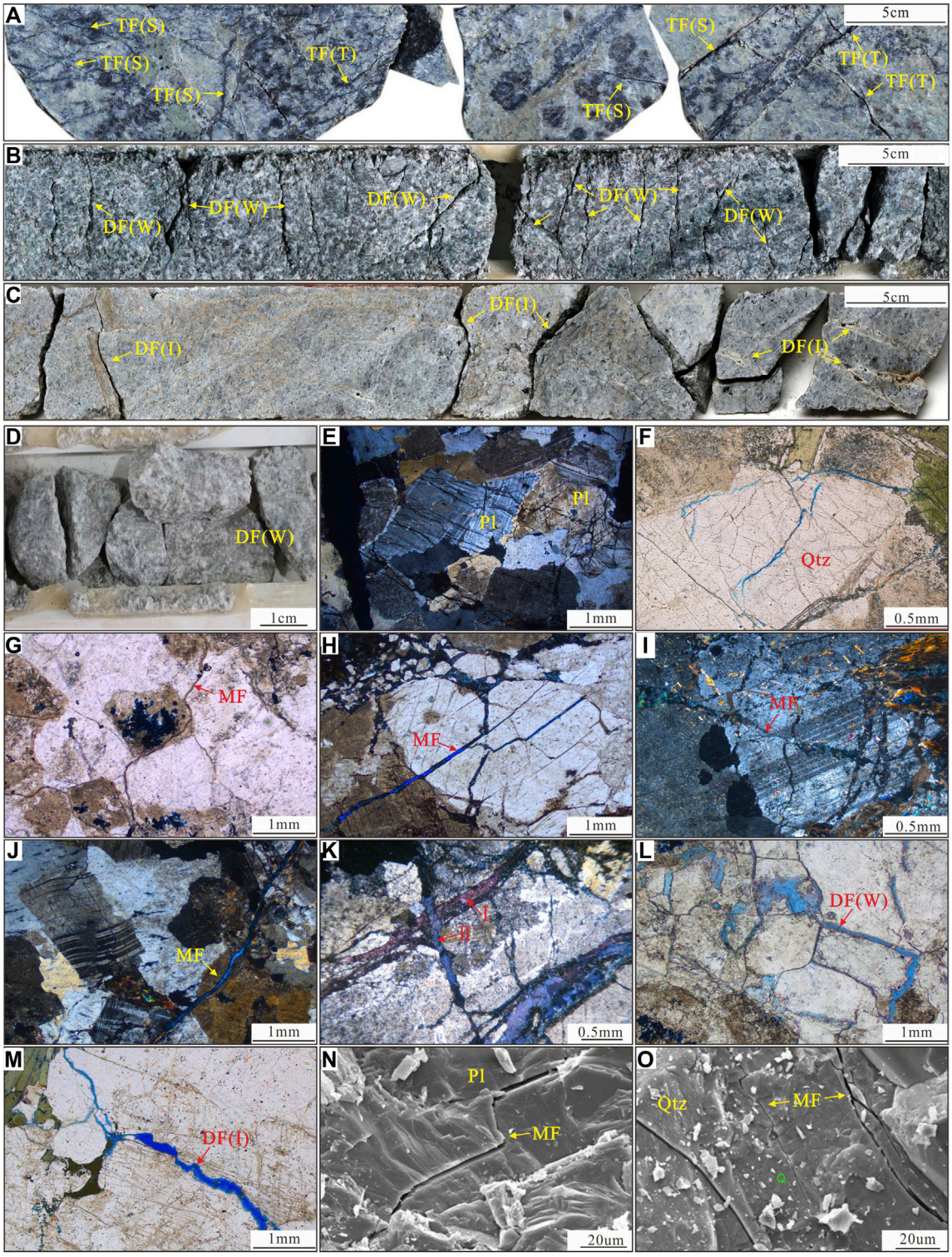

FIGURE 4
Fractures in cores and thin sections. **(A)** Tension fractures and shear fractures in a core, well BZ19-G, 4597.6-4598.1 m; **(B)** Weathering dissolution fractures in a core, well BZ19-G, 4538.3-4538.7 m; **(C)** Inner dissolution fractures in a core, well BZ19-L, 5525.25-5525.70 m; **(D)** Weathering dissolution fractures with strong fragmentation in a core, well BZ19-G, 4538 m; **(E)** Intra-particle fractures in feldspars with regular and straight features, thin section, well BZ19-G, 4599 m; **(F)** Intra-particle fractures in quartz with disorderly cracks, thin section, well BZ19-J, 4614 m; **(G)** Inter-particle fractures, thin section, well BZ19-F, 4487 m; **(H)** Trans-particle fractures, thin section, well BZ19-N, 4497 m; **(I)** Trans-particle fractures directly dissevered the plagioclase bicrystal; thin section, well BZ19-G, 4559 m; **(J)** Trans-particle fractures caused nearby plagioclase twin-crystal bending deformation; thin section, BZ19-G, 4598m; **(K)** Multistage fracture development, thin section, well BZ19-B, 4265 m;
(*Continued*)

FIGURE 4
(L) Weathering dissolution fractures are often distributed in a network, thin section, well BZ19-H, 4584 m; **(M)** Inner dissolution fractures in thin sections, well BZ19-O, 5156 m; **(N)** Intra-particle fractures in feldspars, SEM image, well BZ19-O, 4856 m; **(O)** Intra-particle fractures in quartz, SEM image, well BZ19-M, 4898m; Qtz=quartz, Pl=plagioclase, TF(T)=tension fractures, TF(S)=shear fractures, DF(W) = weathering dissolution fractures, DF(I)=inner dissolution fractures, MF= microfractures).

plagioclase bicrystals (Figure 4I), and nearby plagioclase twin-crystal bending deformation is present (Figure 4J), indicating that the trans-particle fractures formed under shear force. The early fractures are cut by late fractures, indicating that fractures of multiple stages have developed in the study area (Figure 4K).

4.2.2 Dissolution Fractures

The Archean metamorphic rock buried hills have been strongly modified by dissolution associated with geological fluids, and many dissolution fractures developd. According to the source and distribution of the fluids, we subdivide the dissolution fractures into weathering dissolution fractures and inner dissolution fractures.

The top interface of the Archean buried hill in the study area has been strongly modified by weathering and eluviation (Xu et al., 2020), and a large number of low-angle and high-density fractures without obvious directivity are observed in the cores (Figure 4B). These fractures mainly developed at the top of the buried hill near unconformity surfaces in the 50–100 m range, and strong fragmentation is observed (Figure 4D). The weathering dissolution fractures observed in thin sections are often distributed in networks and interlaced with dissolution pores and tectonic fractures (Figure 4L). We define the pre-existing fractures on the tops of buried hill in the study area that formed after dissolution by atmospheric freshwater as weathering dissolution fractures.

Some dissolution fractures are usually found far from the Archean top surface, in this paper, we call these fractures inner dissolution fractures to distinguish them from the weathering dissolution fractures mentioned above. The inner dissolution fractures are mainly fractures formed in the deep part of the buried hill that were modified by dissolution and transformed by organic acid fluids. Fractures are filled by early carbonate minerals that are then dissolved. In the study area, the inner dissolution fractures in the cores have widths of up to 2 mm (Figure 4C). The aperture of the initial fracture is enlarged after dissolution modification (Zhao et al., 2018). The core is "dendritic", and the shape of the fracture wall becomes irregular, unsmooth and serrated (Figure 4C). Although the newly formed fractures have evident corrosion characteristics, the original shapes and distributions of the initial fractures remain distinguishable (Figure 4M).

4.3 Characteristic parameters of fractures

A basic method to study the development degree and distribution of fractures in metamorphic rocks is to measure fracture parameters and statistical fracture filling in cores. According to the observation and analysis of existing core fractures, the results show that tectonic fractures are dominant in the study area, accounting for 71.7% of all fractures, with tension fractures accounting for 16.56% of all fractures and shear fractures accounting for 55.14%. There are relatively few dissolution fractures, which account for 28.3% of all fractures; weathering dissolution fractures account for 24.2%, and inner dissolution fractures account for only 4.1% (Figure 5A). Fractures are developed at low angles (dips of 0°–30°), accounting for 47.75%; moderate angles (dips of 30°–60°) account for 32.35%, and high-angle fractures (dips of 60°–90°) account for 19.9% (Figure 5B). Microscopic, observation reveals that trans-particle fractures account for 53.6% of microfractures, and intra-particle and inter-particle fractures account for 29.7 and 16.7%, respectively (Figure 5E).

The early fractures experienced strong filling, which produced three types of fractures: fully filled (45%), partially filled (23%) and open (32%) (Figure 5C), among which both open fractures and half-filled fractures are effective fractures. The filling materials are mainly composed of ankerite (52.7%), calcite (38.1%) and clay minerals (11.2%) (Figure 5D). The fractures show strong inhomogeneity in the cores, with the average linear densities of fractures ranging from 24 m^{-1} to 56 m^{-1} and with linear density reaching 68 m^{-1} (Figure 5F).

The analysis of the fracture characteristics of the comprehensive columnar section from well BZ19-D (Figure 6) shows that fractures from this single well show obvious changes in the vertical direction. The average linear densities of fractures are calculated by using sine or cosine curves displayed in dynamic images from FMI imaging logs. According to the change in the logging curve from top to bottom, the well is divided into upper and lower parts: the part above 4475 m and the part below 4475 m (Figure 6). The results show that the upper fractures are generally well developed, the dip angles are smaller than those of the lower fractures, and the average linear density of fractures reaches 1.57 m^{-1}. The lower fractures are not as continuously developed as the upper ones, and have an average linear density of 0.98 m^{-1}. However, there are also a few sections with dense fractures. The reasons for the differential development are discussed in the following Section 5.1.

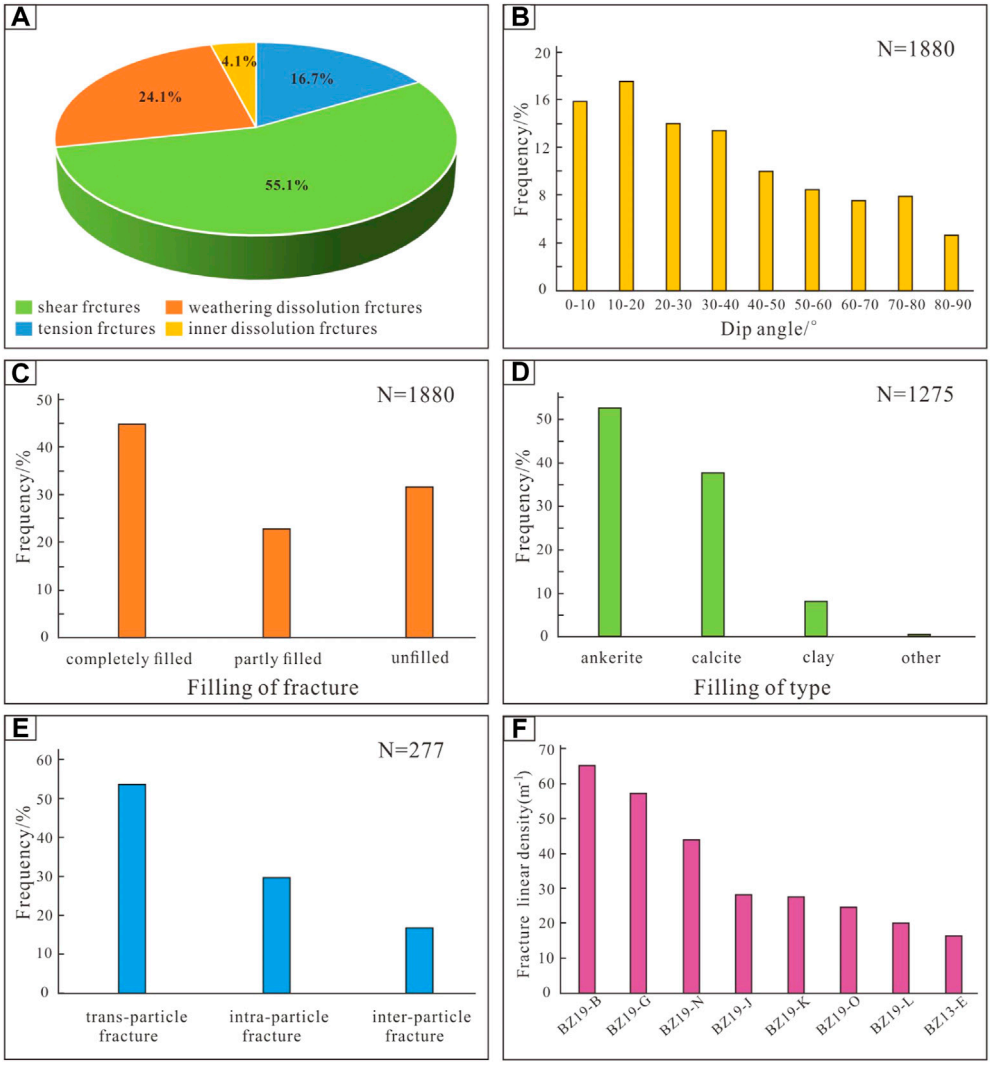

FIGURE 5
Statistical plot of the characteristic parameters of the fractures. **(A)** Statistical results of fracture types in cores; **(B)** Frequency distribution of fracture dip angle in cores; **(C)** Frequency distribution of fracture fillings types in cores; **(D)** Frequency distribution of fracture filling materials in cores; **(E)**. Frequency distribution of microfractures types in thin sections; **(F)** Fracture density of cores in coring wells).

5 Discussion

5.1 Controlling factors of fractures in metamorphic hills

Fracture formation and development in rocks are controlled by both internal and external factors (Ding et al., 2013; Ju and Sun, 2016; Ye et al., 2021b). The internal factors include the lithology, mineral composition and structure of metamorphic rocks. External factors are factors associated with tectonic movement, weathering, and hydrothermal activity (Ding et al., 2012; Zeng et al., 2013).

5.1.1 Lithology

Lithology is the most important internal factor controlling the development of fractures (Ju and Sun, 2016; Wang et al., 2016; Dai et al., 2019; Zheng et al., 2020). Due to the various mineral compositions of different lithologies, the mechanical properties and fracture degrees of rocks significantly vary, which results in great differences in fracture development degree among different rocks under the same stress (Wang et al., 2017).

Migmatization controls the lithological distribution and influences the degree of fractures development in buried hills of metamorphic rocks. Extensive regional metamorphism

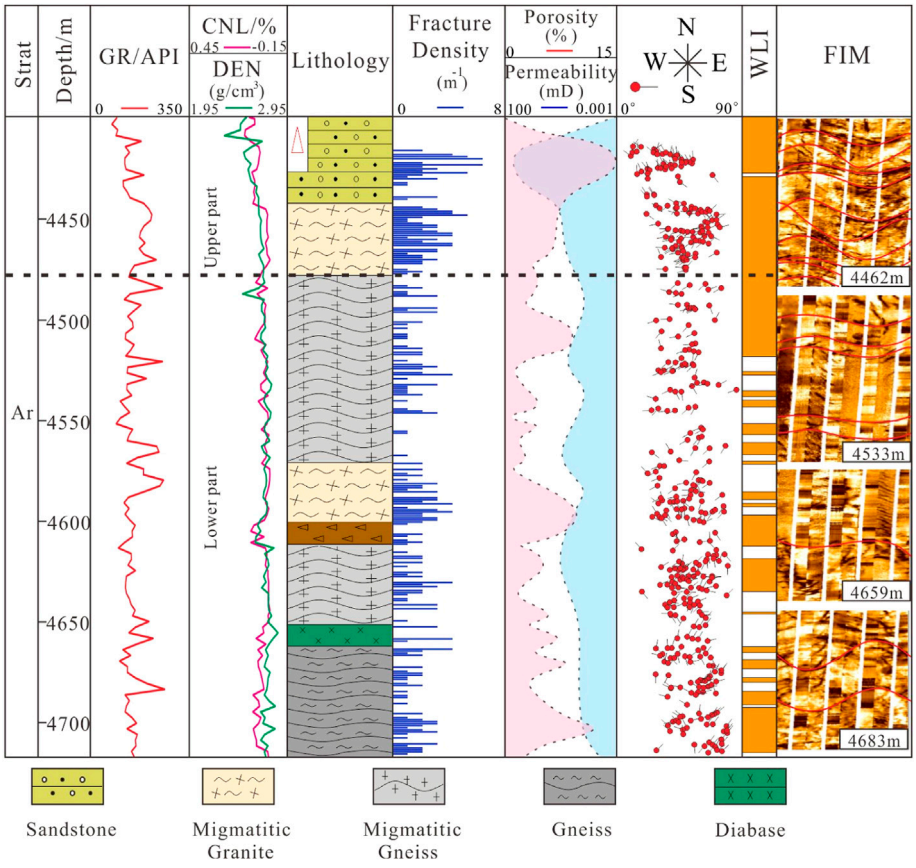

FIGURE 6
Fracture characteristics of the comprehensive columnar section from well BZ19-D.

occurred in the North China Block during 2.55–2.50 Ga (Ye et al., 2021b), and the rocks dominated by TTG underwent strong migmatization under a mantle plume-tectonothermal regime (Geng et al., 2016); as a result, the rocks of Archean buried hill are heterogeneous (Wang and Li, 2014). The degree of migmatization is strongly controlled by the heat source (Vanderhaeghe et al., 1999). Near the heat source, granitic magma is formed by the preferential melting of felsic minerals, and migmatitic granite is formed by ascent, convergence and crystallization. Near the heat source, there are residual melanosomes in the rock, which are mainly migmatitic gneiss. The rock far from the heat source shows the lowest degree of migmatization, and the rock is dominated by melanosomes, which are rich in iron and magnesium minerals such as biotite, and gneissic structure has developed.

The statistical analysis of core fracture density indicates significant differences in the degree of fracture development among various lithologies (Figure 7E). The average linear densities of fractures are highest in migmatitic granite at 60 m^{-1} (Figure 7A), followed by migmatitic gneiss and gneiss at 45 m^{-1} and 27 m^{-1}, respectively (Figures 7B,C), whereas the average linear densities of fractures are least developed in diabase at only 10 m^{-1} (Figure 7D). In addition, fracture density statistics based on imaging logging data confirm that fractures are most densely developed in migmatitic granite, and significantly less developed in gneiss and diabase than in migmatitic gneiss (Figure 6, Figure 8).

As feldspar has two cleavage directions, it is a brittle mineral and easily fractures under stress. Quartz is also subject to rupture under strong stress (Guo and Zhang, 2014; Li et al., 2016); however, biotite and amphibole have good ductility, strong plasticity and poor brittleness, and are more susceptible to bending deformation than feldspar and quartz and difficult to fracture under stress (Jarvie et al., 2007). Previous triaxial stress experiments on Archean metamorphic rocks from the Bohai Bay Basin have shown that rocks rich in felsic minerals have higher Poisson's ratios (mostly above 0.25) and lower elastic moduli (20–30 GPa) and thus have lower compressive strengths and are more prone to fractures than mafic rocks (Ye et al., 2022). Compared with the other metamorphic rocks in the buried hills of the Bohai Bay Basin, the migmatitic granites are more

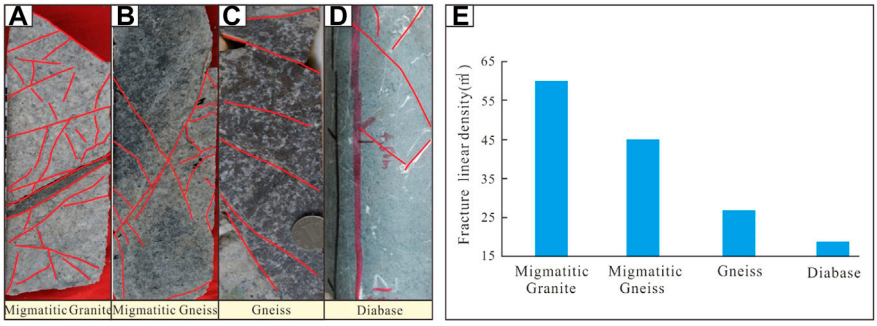

FIGURE 7
(A) Fracture linear densities of migmatitic granite core; **(B)** Fracture linear densities of migmatitic gneiss core; **(C)** Fracture linear densities of gneiss core; **(D)** Fracture linear densities of diabase core; **(E)** Schematic diagram comparing linear densities of fractures in different lithologies.

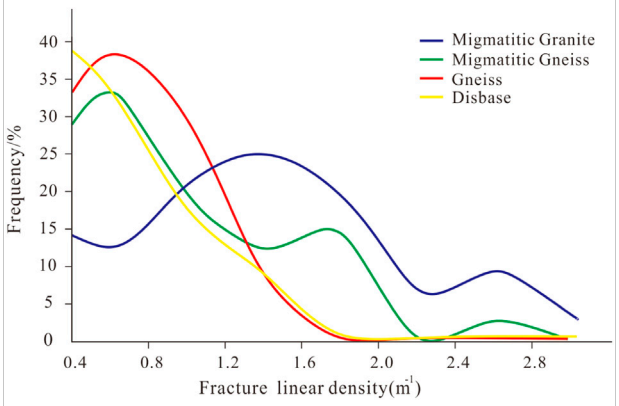

FIGURE 8
The fracture linear densities of different lithologies of Archaean buried hill in the study area obtained from imaging logging data.

likely to be broken and to develop more fractures under the same stress because they have the highest degree of migmatization and high brittleness (Maréchal et al., 2004; Ding et al., 2012; Lander and Laubach, 2015; Li et al., 2017; Li, 2022). Furthermore, the uneven distribution of lithologies and mineral contents results from migmatization; hence, the heterogeneity of the rock mass in the study area is enhanced and leads to the uneven distribution of the stress field inside the rock. These phenomena have contributed to the complexity of fracture development in the study area.

5.1.2 Tectonic movement

Strong tectonic activity and stress conditions control the nature, occurrence and scale of fracture development in buried hills, and thus are important external factors that affect fractures in rocks (Yin et al., 2019).

5.1.2.1 Tectonic Stress Field

The Archean basement in the study area has been controlled by many strong tectonic stress fields, including the Indosinian, Yanshanian and Himalayan tectonic movements, which formed a structural system with mainly normal faults and partially developed strike-slip faults (Li et al., 2010). Influenced by the collision between the South China plate and the North China Plate during the Indosinian period, a series of NWW-oriented thrusting folds and NW-oriented to nearly E-W oriented faults formed in the Bozhong area under NE-SW oriented compression (Cheng et al., 2018) (Figure 9, Figure 10). These faults dip to the south and have a gentle bottom in seismic profiles (Figure 10). The Yanshanian period was influenced by oblique subduction of the Paleo-Pacific plate beneath the Eurasian plate and deep mantle upwelling (Cui et al., 2020). The study area was controlled by a NW-oriented left-spinning torsional stress field (Hou et al., 1998; Cao et al., 2015), under which many nearly NE-oriented compressional-torsional faults and strike-slip faults developed (Figure 9). Meanwhile, the existing reverse faults were negatively reversed under back-arc extensional stress, controlling the Mesozoic stratigraphic deposition. In the late Yanshanian period, differential uplift occurred in the study area due to NW-oriented re-extrusion, which caused the BZ19-6 block to be significantly uplifted and the Mesozoic strata to be completely eroded (Figure 10). Because of the decrease in rock strength after rupture, the pre-existing nearly E-W oriented faults of the Indosinian period and the NNE-oriented faults of the Yanshanian period had different degrees of extensional activation under the strong S-N oriented extensional action during the Himalayan period, improving the effectiveness of the faults (Wang et al., 2018).

5.1.2.2 Control of faults on fractures

Many scholars have examined the relationship between faults and fractures and found that faults control the development of

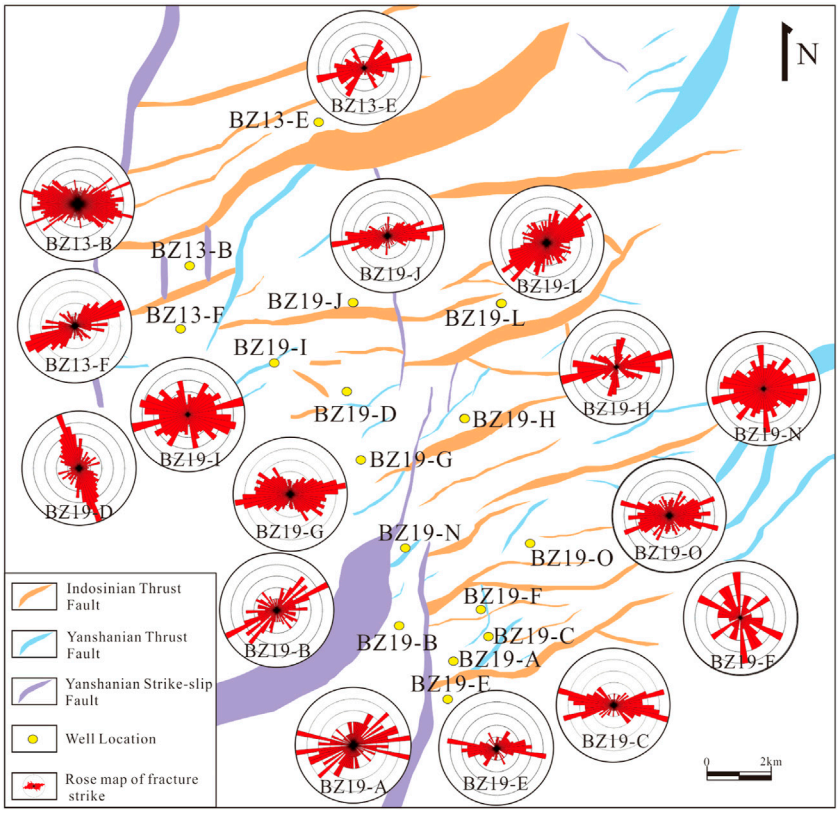

FIGURE 9
Directions of faults and fractures in the metamorphic rocks of the study area. The faults shown in this figure are the larger major faults in the study area. Fault data are modified from Xue et al., 2021 and fracture orientations are derived from the imaging logs of 16 wells.

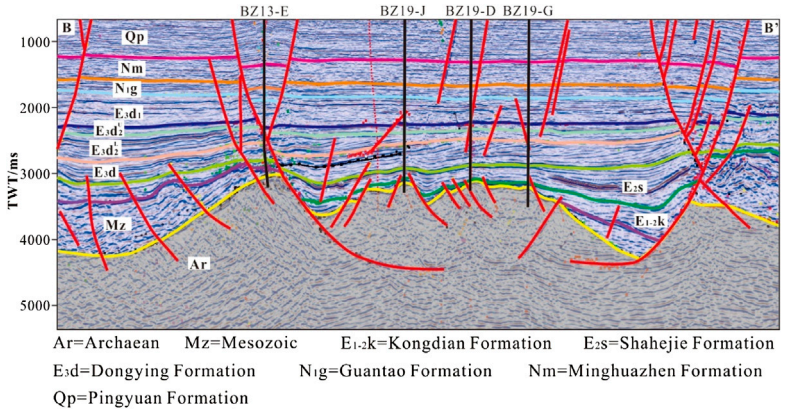

FIGURE 10
Characteristics of the seismic profile along the B-B′ line in the study area (Profile position is shown in Figure 1B). A–A′ represents the profile position of Figure1C and B–B′ represents the profile position of Figure10.

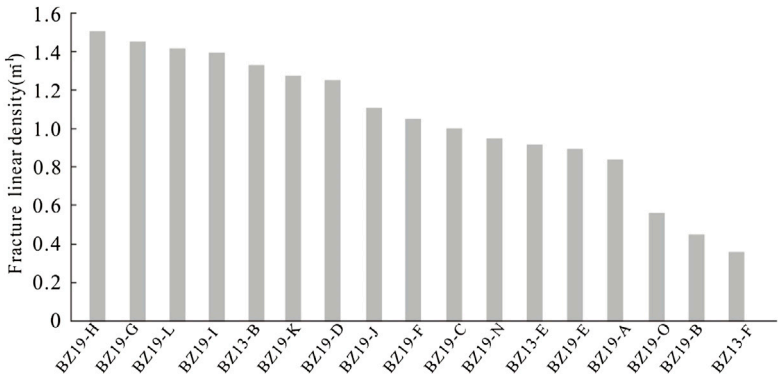

FIGURE 11
Histogram of fracture linear density for different wells in the study area (Fracture linear density is derived from the imaging logs of 17 wells).

fractures by influencing the surrounding tectonic stress strength (Kim et al., 2000; Yin and Wu, 2020; Lan et al., 2021). Ding et al. (2012) and Lyu et al. (2019) concluded that the development of fractures is mainly related to the distance to the fault, with the degree of fracture development decreasing with increasing distance from the fault. In the study area, due to the complex tectonic movement and the simultaneous production of a large number of fractures, the fracture development in each well is controlled by multiple nearby faults, so the relationship between fracture density and fault distance cannot be well shown. However, according to a rose diagram of fracture trends in 16 exploration wells, the orientation of tectonic fractures is mainly parallel or almost parallel to the orientation of adjacent faults, which shows that faults play an important role in fracture development. During the Indosinian period, the local stress caused by NE to nearly E-W oriented faults caused fractures to develop parallel to the fault direction. The development of a large number of nearly E-W oriented fractures in the study area indicates that the local stress of the faults generated under the strong compression and thrust was strong in the Indosinian period, which was the key period for the large-scale development of fractures. Moreover, as shown by wells BZ19-A, BZ19-B, BZ13-F, BZ19-H and BZ19-N, many NE-oriented fractures are developed and parallel to the adjacent NE-oriented faults, which proves that the local stress caused by NE-oriented faults in the Yanshanian period also produce some fractures (Figure 9). In addition, fracture density is partially controlled by the fracture effect (Souque et al., 2019). Wells BZ19-C, BZ19-F, and BZ19-H are located at the intersections of multiple fault zones (Figure 9), resulting in stress release centrally and a fracture density as high as 1.5 m^{-1}. (Figure 11). It should be noted that although the lithology of wells BZ19-C and BZ19-F is gneiss, they have high fracture densities, which shows that the controlling effect of tectonics on fractures is greater than that of lithology in the study area.

5.1.3 Fluid modification

The effect of dissolution on fracture improvement is obvious (Ye et al., 2020a). Fractures generated in the early stage provide effective migration pathways for fluids. The circulation of fluids promotes the evolution of the water–rock system, material migration and enrichment. These processes lead to a series of transformation reactions between minerals (Dou et al., 2010) and promotes fracture modification.

Metamorphic rock dissolution is mainly controlled by two types of fluids: atmospheric freshwater during the surface exposure period and organic acids and carbon dioxide generated by the thermal evolution of organic matter during the burial period (Ye et al., 2022). During this process, atmospheric freshwater dissolves and hydrates calcium carbonate minerals as well as silicate and aluminosilicate minerals in rocks to generate clay minerals such as illite, kaolinite and chlorite (Tan et al., 2014; Hong et al., 2020), and the original tectonic fractures expand and dissolve to form weathering dissolution fractures (Figure 12A). These fractures are interlaced with dissolution pores and tectonic fractures (Figure 4L). Furthermore, the study area was laterally docked with the hydrocarbon source rocks of the Shahejie Formation; therefore, the organic acids and carbon dioxide produced by the mature hydrocarbon source rocks of the Shahejie Formation migrated into the fractures of the inner buried hill. The unstable minerals (such as calcite and ankerite) filling the early fractures were again dissolved under the action of organic acids (Figure 12B). Thus, inner dissolution fractures were formed, which enhanced fracture effectiveness (Giammar et al., 2005; Aminul Islam, 2009; Liu et al., 2022). In this process, local tectonic fractures improved the

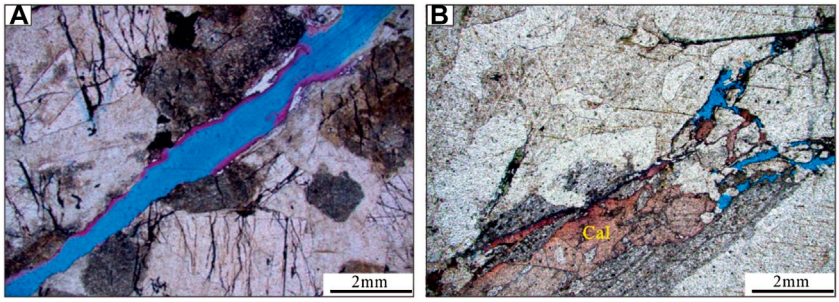

FIGURE 12
Dissolution fractures in thin sections of metamorphic rocks in the study area **(A)** Early tectonic fractures exhibiting corrosion and expansion, well BZ19-G, 4599 m; **(B)** The mineral of calcite in the filling fracture is partially dissolved, which makes the initial fracture effective, BZ13-G,4732 m).

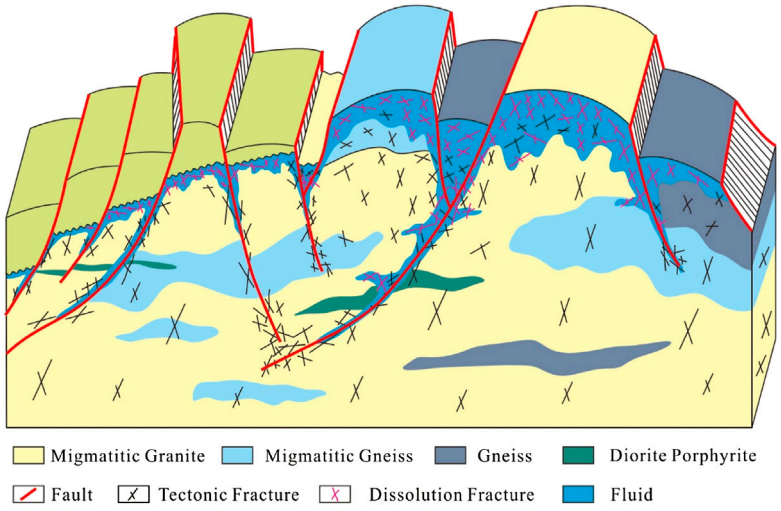

FIGURE 13
The distribution pattern of fractures in buried hill of metamorphic rocks.

permeability of the reservoir, enhanced the fluidity of the fluid, and facilitated dissolution. The existing dissolution pores and fractures made the reservoir more prone to producing fractures under the action of tectonic stress, and the two processes complemented each other.

In general, stronger dissolution occurred within the weathering crust near the tops of buried hill, and dissolution in the inner buried hill was mainly controlled by the development of fractures. All kinds of minerals near the fractures show obvious alteration characteristics (You et al., 2021), while with increasing distance far from the fractures, the degree of alteration obviously weakens until gradually transforming into normal rock without alteration. This phenomenon has been confirmed by thin section observation and mineral diffraction studies as part of the exploration of buried hill in the PL nine to one oilfield (Wang et al., 2015).

5.2 Fracture development pattern

The fracture development of buried hill in the study area varies significantly in the vertical direction due to the superposition of rock lithology, tectonic stress and later fluid modification. Here, the above controlling factors are used to establish a "native influence, multiphase superposition, fluid modification" model of fracture development in buried hill of metamorphic rocks (Figure 13).

The main rock type in the study area is migmatitic granite, which has more brittle minerals than gneiss, laying a good foundation for the development of fractures. The strong compressional collision during the Indosinian and the left-lateral strike-slip and thrust activities during the Yanshanian provided external conditions favourable for fracture formation. Under their combined effects, multiple phase fractures were

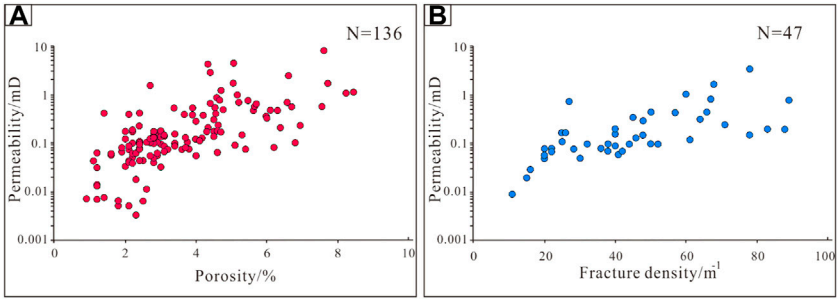

FIGURE 14
Physical property relationships of buried hill reservoir core samples in the study area. **(A)** The relationship between porosity and permeability; **(B)** The relationship between permeability and fracture linear density).

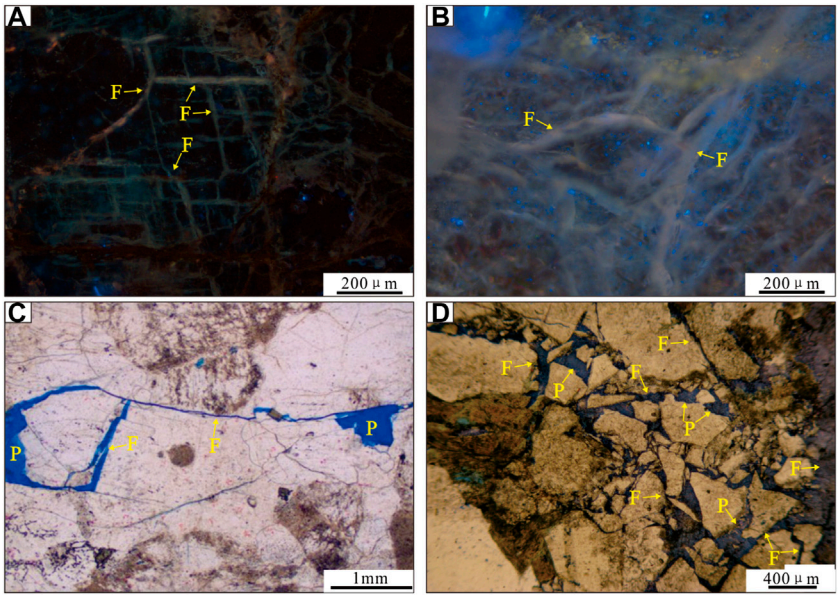

FIGURE 15
Thin-section photomicrographs and fluorescence scanning photos showing fractures and pores in the Archean metamorphic rocks in the study area. **(A)** Fractures in migmatitic granite under fluorescence scanning photos, show significant oil and gas displays, BZ19-G, 4544 m; **(B)** Fractures in migmatitic gneiss under fluorescence scanning photos, show significant oil and gas displays, BZ13-E, 4628 m; **(C)** Fractures act as channels to connect the secondary pores BZ19-J, 4903 m; **(D)** Secondary pores develop along the fractures, BZ19-B, 4432 m; P = secondary pore, F = fracture).

superimposed, resulting in the formation of many tectonic fractures in buried hills. In the stress concentration areas, such as the sides of faults and intersections, "mesh-like" fracture dense zones formd. Influenced by the differential uplift between the Indosinian and Yanshanian periods, the high part of the buried hill experienced strong weathering and erosion. The openings of the existing tectonic fractures near the top of the buried hill enlarged and formed a "layered" weathering fracture zone under the action of atmospheric freshwater dissolution. The reservoir space was dominated by weathering dissolution fractures, and a few dissolution pores were also developed. The absence of Mesozoic strata in the BZ19-6 block, in contrast to the BZ13-2 block, reflects the longer exposure time and thicker weathering fracture zone development in the former block. The Himalayan tectonic movement reactivated the fractures that were closed and filled earlier. The pre-existing faults and unconformities are the weak zones in buried hill and the dominant pathways for fluid

migration in the later stage. The organic acids and carbon dioxide produced by the mature hydrocarbon source rocks of the Shahejie Formation were transported to the inner buried hill, and the primary fractures around the faults were enlarged through dissolution to form dendritic inner dissolution fractures. This process is key to the development of effective fractures in buried hill; however, it is difficult for fractures to develop in areas far from faults or where gneiss is present.

5.3 Contributions of fractures to reservoir quality

The basement reservoirs of the Archean metamorphic rocks in the Bohai Bay Basin have experienced transformations and processes such as metamorphic recrystallization, weathering, dissolution, and tectonic disruption over a long geological period, developing storage space that is complex and heterogeneous (Luo et al., 2005). The basement petrophysical properties of 136 samples were statistically analysed according to the degree of fracture development (Figure 14A). The reservoir physical properties in the study area vary widely, with porosity mainly between 2 and 8% and permeability between 0.1×10^{-3} μm^2 and 1×10^{-3} μm^2. Further statistics on the relationship between fracture density and physical properties show that fracture density is positively correlated with permeability (Figure 14B), indicating that fractures contribute significantly to reservoir physical properties. Furthermore, we observe in thin sections that most dissolution pores do not exist in isolation but are connected by fractures (Figures 15C,D), which is conducive to the formation of effective reservoir space and enhancement of basement reservoir properties. However, except for some samples with strong fragmentation, the rocks with obvious fracture development observed in many thin sections do not have high porosity (Figure 4J). Migmatite has close to no primary porosity, and its porosity is mainly controlled by later dissolution. Fractures provide migration channels for later erosive fluids (such as organic acids and CO_2), and only rocks superimposed with dissolution can develop higher porosity. Therefore, the influence of fractures on rock porosity is indirectly controlled, and the formation of high porosity rocks is related to the configuration of the source and migration path of erosive fluids (such as unconformities, source rocks, and deep and large faults). In addition, in the core fluorescence scanning images, oil and gas are clearly present in these fractures (Figures 15A,B), which implies that fractures can provide effective space for oil and gas storage and/or migration pathways for later oil and gas seepage (Ding et al., 2013; Guo et al., 2016). These results imply that the development degree of fractures determines the distribution of favourable reservoirs (Zeng and Li, 2009).

6 Conclusion

1) Fractures in the study area can be divided into two genetic types: tectonic fractures and dissolution fractures. Tectonic fractures can be divided into tension fractures, shear fractures and microfractures, while dissolution fractures include weathering dissolution fractures and inner dissolution fractures. Tectonic fractures are widely developed in the study area. There is obvious variation in the degree of fracture development in the vertical direction within single wells.
2) Fracture development is controlled by lithology, tectonics and fluid activity. The migmatitic granite is the most favourable lithology for fracture development, having a higher content of brittle minerals than other lithologies. The Indosinian and Yanshanian were key periods for the development of fractures due to tectonic movements in the study area, and the pre-existing fractures are reactivated during the Himalayan period. Organic acids and CO_2 generated by the thermal evolution of atmospheric freshwater and organic matter are dissolved along the fractures.
3) Fracture-intensive zones are the main development sites for hydrocarbon reservoirs, which enhance the porosity and permeability of buried hill of Archean metamorphic rocks and provide effective space for oil and gas storage and migration. They play an important role in the formation of large-scale reservoirs.

Data availability statement

The original contributions presented in the study are included in the article/supplementary material, further inquiries can be directed to the corresponding author.

Author contributions

WW is responsible for the idea, writing and revision of this paper. WW, XZ, XL, PL and XR are responsible for the data analysis and drawing. XS and JY is responsible for reviewing and editing.

Funding

National Natural Science Foundation of China (No. 41790453, No. 41972313); Science and Technology Department Project of Jilin Province (Grant No.20200403068SF, 20210101108JC).

Conflict of interest

Authors XZ and XL were employed by the Tianjin Branch of China National Offshore Oil Corporation.

The authors declare that the research was conducted in the absence of any commercial or financial relationships that could be construed as a potential conflict of interest.

Publisher's note

References

Achtziger-Zupančič, P., Loew, S., and Hiller, A. (2017). Factors controlling the permeability distribution in fault vein zones surrounding granitic intrusions (Ore Mountains/Germany). *J. Geophys. Res. Solid Earth* 122 (3), 1876–1899. doi:10.1002/2016JB013619

Allen, M. B., Macdonald, D. I. M., Xun, Z., Vincent, S. J., and Brouet-Menzies, C. (1997). Early Cenozoic two-phase extension and late Cenozoic thermal subsidence and inversion of the Bohai Basin, northern China. *Mar. Petroleum Geol.* 14 (7-8), 951–972. doi:10.1016/S0264-8172(97)00027-5

Ameen, M. S., Buhidma, I. M., and Rahim, Z. (2010). The function of fractures and *in-situ* stresses in the Khuff reservoir performance, onshore fields, Saudi Arabia. *Bulletin* 94 (1), 27–60. doi:10.1306/06160909012

Aminul Islam, M. (2009). Diagenesis and reservoir quality of bhuban sandstones (Neogene), titas gas field, bengal basin, Bangladesh. *J. Asian Earth Sci.* 35 (1), 89–100. doi:10.1016/j.jseaes.2009.01.006

Aydin, A. (2000). Fractures, faults, and hydrocarbon entrapment, migration and flow. *Mar. Petroleum Geol.* 17 (7), 797–814. doi:10.1016/S0264-8172(00)00020-9

Bazalgette, L., Petit, J.-P., Amrhar, M., and Ouanaïmi, H. (2010). Aspects and origins of fractured dip-domain boundaries in folded carbonate rocks. *J. Struct. Geol.* 32 (4), 523–536. doi:10.1016/j.jsg.2010.03.002

Cao, X. Z., Li, S. Z., Xu, L. Q., Guo, L. L., Liu, L. P., Zhao, S., et al. (2015). Mesozoic–Cenozoic evolution and mechanism of tectonic geomorphology in the central North China Block: Constraint from apatite fission track thermochronologyfission track thermochronology. *J. Asian Earth Sci.* 114 (1), 41–53. doi:10.1016/j.jseaes.2015.03.041

Carvalho, I. de S., Mendes, J. C., and Costa, T. (2013). The role of fracturing and mineralogical alteration of basement gneiss in the oil exhsudation in the Sousa Basin (Lower Cretaceous), Northeastern Brazil. *J. S. Am. Earth Sci.* 47, 47–54. doi:10.1016/j.jsames.2013.06.001

Chen, G. B., Li, T., Yang, L., Zhang, G. H., Li, J. W., and Dong, H. J. (2021). Mechanical properties and failure mechanism of combined bodies with different coal-rock ratios and combinations. *J. Min. Strata Control Eng.* 3 (2), 023522. doi:10.13532/j.jmsce.cn10-1638/td.20210108.001

Cheng, Y. J., Wu, Z. P., Lu, S. N., Li, X., Lin, C. Y., Huang, Z., et al. (2018). Mesozoic to cenozoic tectonic transition process in zhanhua sag, Bohai Bay Basin, east China. *Tectonophysics* 730 (1), 11–28. doi:10.1016/j.tecto.2018.02.010

Cui, F. H., Xu, X. U., Zheng, C. Q., Yao, W. G., and Shi, L. (2020). The paleo-Pacific plate subduction and slab roll-back beneath eastern North China Craton: Insights from the Late Mesozoic granitoids in Xingcheng area, Western Liaoning Province. *Acta Petrol. Sin.* 36 (8), 2463–2492. doi:10.18654/1000-0569/2020.08.12

Cui, J. D., Zhang, J. Z., and Zhang, H. Y. (2013). Features of the carboniferous volcanic rocks fracture reservoirs in Hongshanzui oilfield, Junggar Basin. *J. Earth Sci.* 24 (6), 997–1007. doi:10.1007/s12583-013-0397-z

Cuong, T. X., and Warren, J. K. (2009). Bach ho field, a fractured granitic basement reservoir, cuu long basin, offshore se vietnam: a "buried-hill" play. *J. Petroleum Geol.* 32 (2), 129–156. doi:10.1111/j.1747-5457.2009.00440.x

Dai, X. J., Tang, H. F., Zhang, T., Zhao, P. J., Xu, C. M., Kong, T., et al. (2019). Facies architecture model of the shimentan formation pyroclastic rocks in the block-T units, xihu sag, east China sea basin, and its exploration significance. *Acta Geol. sinica-. Engl. Ed.* 93 (4), 1076–1087. doi:10.1111/1755-6724.13807

Ding, W. L., Li, C., Li, C. Y., Xu, C. C., Jiu, K., Zeng, W. T., et al. (2012). Fracture development in shale and its relationship to gas accumulation. *Geosci. Front.* 3 (1), 97–105. doi:10.1016/j.gsf.2011.10.001

Ding, W. L., Zhu, D. W., Cai, J. J., Gong, M. L., and Chen, F. Y. (2013). Analysis of the developmental characteristics and major regulating factors of fractures in marine-continental transitional shale-gas reservoirs: A case study of the carboniferous-permian strata in the southeastern ordos basin, central China. *Mar. Petroleum Geol.* 45, 121–133. doi:10.1016/j.marpetgeo.2013.04.022

Dou, L. R., Wei, X. D., Wang, J. C., Li, J. L., and Zhang, S. H. (2015). Characteristics of granitic basement rock buried-hill reservoir in Bongor Basin, Chad. *Acta Pet. Sin.* 36 (8), 897–904,925. doi:10.7623/syxb201508001

Dou, S. M., Chen, F. R., Yang, Y. Q., W, S. J., Kang, M. L., and Zhang, R. (2010). Estimation of saturation index for the precipitation of secondary minerals during water-rock interaction in granite terrains. *Geochimica* 39 (4), 326–336. doi:10.19700/j.0379-1726.2010.04.004

Eig, K., and Bergh, S. G. (2011). Late Cretaceous-Cenozoic fracturing in Lofoten, North Norway: Tectonic significance, fracture mechanisms and controlling factors. *Tectonophysics* 499 (1-4), 190–205. doi:10.1016/j.tecto.2010.12.002

Fu, Q., You, Y. C., and Wu, Z. (2003). Tectonic episodes and reservoir fissure systems in Caotai metamorphic. *buried hill Reserv.* 30 (5), 18–20. doi:10.3321/j.issn:1000-0747.2003.05.005

Geng, Y. S., Shen, Q. H., Du, L. L., and Song, H. X. (2016). Regional metamorphism and continental growth and assembly in China. *Acta Petrol. Sin.* 32 (9), 2579–2608. CNKI:SUN:YSXB.0.2016-09-001.

Giammar, D. E., Jr, R. G. B., and Peters, C. A. (2005). Forsterite dissolution and magnesite precipitation at conditions relevant for deep saline aquifer storage and sequestration of carbon dioxide. *Chem. Geol.* 217 (3), 257–276. doi:10.1016/j.chemgeo.2004.12.013

Guo, P., Yao, L. H., and Ren, D. S. (2016). Simulation of three-dimensional tectonic stress fields and quantitative prediction of tectonic fracture within the Damintun Depression, Liaohe Basin, northeast China. *J. Struct. Geol.* 86, 211–223. doi:10.1016/j.jsg.2016.03.007

Guo, T. L., and Zhang, H. R. (2014). Formation and enrichment mode of Jiaoshiba shale gas field, Sichuan Basin. *Petroleum Explor. Dev.* 41 (1), 31–40. doi:10.1016/s1876-3804(14)60003-3

Guo, Y., Wang, Y. C., Wei, A. J., Wu, H. M., Ye, T., Gao, K. S., et al. (2017). Characteristics and controlling factors of volcanic reservoir in buried hill -- a case study of Cretaceous in Qinhuangdao 30A area in Bohai Sea Area. *Acta Sedimentol. Sin.* 35 (2), 343–357. doi:10.14027/j.cnki.cjxb.2017.02.012

Han, C. C., Tian, J. J., Hu, C. L., Liu, H. L., Wang, W. F., Huan, Z., et al. (2020). Lithofacies characteristics and their controlling effects on reservoirs in buried hills of metamorphic rocks: A case study of late paleozoic units in the Aryskum depression, South Turgay basin, Kazakhstan. *J. Petroleum Sci. Eng.* 191 (0), 107137. doi:10.1016/j.petrol.2020.107137

Hong, D., Cao, J., Wu, T., Dang, S., Hu, W., and Yao, S. (2020). Authigenic clay minerals and calcite dissolution influence reservoir quality in tight sandstones: Insights from the central Junggar Basin, NW China. *Energy Geosci.* 1 (1–2), 8–19. doi:10.1016/j.engeos.2020.03.001

Hou, G. T., Qian, X. L., and Cai, D. S. (2001). The tectonic evolution of Bohai basin in mesozoic and cenozoic time. *Acta Sci. Nat. Univ. Pekin.* 37 (6), 845–851. doi:10.3321/j.issn:0479-8023.2001.06.016

Hou, G. T., Qian, X. L., and Song, X. M. (1998). Study on formation mechanism of Bohai Bay Basin. *Acta Sci. Nat. Univ. Pekin.* 34 (4). doi:10.13209/j.0479-8023.1998.033

Hou, M. C., Cao, H. Y., Li, H. Y., Chen, A. Q., and Wei, A. J. (2019). Characteristics and controlling factors of deep buried-hill reservoirs in the BZ19-6 structural belt, Bohai sea area. *Nat. Gas. Ind.* 39 (1), 33–44. doi:10.3787/j.issn.1000-0976.2019.01.004

Jarvie, D. M., Hill, R. J., Ruble, T. E., and Pollastro, R. M. (2007). Unconventional shale-gas systems: The Mississippian Barnett Shale of north-central Texas as one model for thermogenic shale-gas assessment. *Am. Assoc. Pet. Geol. Bull.* 91 (4), 475–499. doi:10.1306/12190606068

Ju, W., and Sun, W. F. (2016). Tectonic fractures in the lower cretaceous xiagou formation of qingxi oilfield, jiuxi basin, NW China part one: Characteristics and controlling factors. *J. Petroleum Sci. Eng.* 146, 617–625. doi:10.1016/j.petrol.2016.07.042

Kim, Y.-S., Andrews, J. R., and Sanderson, D. J. (2000). Damage zones around strike-slip fault systems and strike-slip fault evolution, Crackington Haven, southwest England. *Geosci. J.* 4 (2), 53–72. doi:10.1007/BF02910127

Lai, J., Li, D., Wang, G. W., Xiao, C. W., Hao, X. L., Luo, Q., et al. (2019). Earth stress and reservoir quality evaluation in high and steep structure: The Lower Cretaceous in the Kuqa Depression, Tarim Basin, China. *Mar. Petroleum Geol.* 101, 43–54. doi:10.1016/j.marpetgeo.2018.11.036

Lan, S. R., Song, D. Z., Li, Z. L., and Liu, Y. (2021). Experimental study on acoustic emission characteristics of fault slip process based on damage factor. *J. Min. Strata Control Eng.* 3 (3), 033024. doi:10.13532/j.jmsce.cn10-1638/td.20210510.002

Lander, R. H., and Laubach, S. E. (2015). Insights into rates of fracture growth and sealing from a model for quartz cementation in fractured sandstones. *Geol. Soc. Am. Bull.* 127 (3-4), 516–538. doi:10.1130/B31092.1

Li, A., Ding, W. L., He, J. H., Dai, P., Yin, S., and Xie, F. (2016). Investigation of pore structure and fractal characteristics of organic-rich shale reservoirs: A case study of lower cambrian qiongzhusi formation in malong block of eastern yunnan province, south China. *Mar. Petroleum Geol.* 70, 46–57. doi:10.1016/j.marpetgeo.2015.11.004

Li, A., Ding, W. L., Wang, R. Y., He, J. H., Wang, X. H., Sun, Y., et al. (2017). Petrophysical characterization of shale reservoir based on nuclear magnetic resonance (nmr) experiment: A case study of lower cambrian qiongzhusi formation in eastern yunnan province, south China. *J. Nat. Gas Sci. Eng.* 37, 29–38. doi:10.1016/j.jngse.2016.11.034

Li, H., Qin, Q., Zhang, B. J., Ge, X. Y., Hu, X., Fan, C. H., et al. (2020). Tectonic fracture formation and distribution in ultradeep marine carbonate gas reservoirs: A case study of the maokou formation in the jiulongshan gas field, sichuan basin, southwest China. *Energy fuels.* 34 (11), 14132–14146. doi:10.1021/acs.energyfuels.0c03327

Li, H. (2022). Research progress on evaluation methods and factors influencing shale brittleness: A review. *Energy Rep.* 8, 4344–4358. doi:10.1016/j.egyr.2022.03.120

Li, S. Z., Suo, Y. H., Dai, L. M., Liu, L. P., Jin, C., and Liu, X. (2010). formation of Bohai Bay Basin and destruction of north China craton. *Earth Sci. Front.* 17 (4), 064–089. CNKI:SUN:DXQY.0.2010-04-009.

Li, S. Z., Suo, Y. H., Santosh, M., Dai, L. M., Liu, X., Yu, S., et al. (2013). Mesozoic to cenozoic intracontinental deformation and dynamics of the north China craton. *Geol. J.* 48 (5), 543–560. doi:10.1002/gj.2500

Li, W., Dou, L. R., Wen, Z. G., Zhang, G. Y., and Hu, Y. (2017). Buried-hill hydrocarbon Genesis and accumulation process in Bongor Basin, Chad. *Acta Pet. Sin.* 38 (11), 1253–1262. doi:10.7623/syxb201711004

Li, X., Yan, W. P., Cui, Z. Q., Guo, B. C., Liang, K., and Tao, Z. (2012). Prospecting potential and targets of buried-hill oil and gas reservoirs in Bohai Bay Basin. *Petroleum Geol. Exp.* 34 (2), 140–139. doi:10.11781/sysydz201202140

Li, Y., Hou, G. T., Hari, K. R., Neng, Y., Lei, G. L., Tang, Y., et al. (2018). The model of fracture development in the faulted folds: The role of folding and faulting. *Mar. Petroleum Geol.* 89, 243–251. doi:10.1016/j.marpetgeo.2017.05.025

Li, Y., Zhou, D., Wang, W., Jiang, T., and Xue, Z. (2020). Development of unconventional gas and technologies adopted in China. *Energy Geosci.* 1 (1–2), 55–68. doi:10.1016/j.engeos.2020.04.004

Liang, J. T., Wang, H. L., Bai, Y., Ji, X. Y., and Duo, X. M. (2016). Cenozoic tectonic evolution of the Bohai Bay Basin and its coupling relationship with Pacific plate subduction. *J. Asian Earth Sci.* 127, 257–266. doi:10.1016/j.jseaes.2016.06.012

Liu, C., Xie, Q. B., Wang, G. W., Zhang, C. J., Wang, L. L., and Qi, K. N. (2016). Reservoir properties and controlling factors of contact metamorphic zones of the diabase in the northern slope of the Gaoyou Sag, Subei Basin, eastern China. *J. Nat. Gas Sci. Eng.* 35, 392–411. doi:10.1016/j.jngse.2016.08.070

Liu, G. P., Zeng, L. B., Li, H. G., Ostadhassan, M., and Rabiei, M. (2020). Natural fractures in metamorphic basement reservoirs in the Liaohe Basin, China. *Mar. Petroleum Geol.* 119, 104479. doi:10.1016/j.marpetgeo.2020.104479

Liu, Y., Chen, L., Tang, Y., Zhang, X., and Qiu, Z. (2022). Synthesis and characterization of nano-SiO2@octadecylbisimidazoline quaternary ammonium salt used as acidizing corrosion inhibitor. *Rev. Adv. Mater. Sci.* 61 (1), 186–194. doi:10.1515/rams-2022-0006

Luo, J. L., Morad, S., Liang, Z. G., and Zhu, Y. S. (2005). Controls on the quality of Archean metamorphic and Jurassic volcanic reservoir rocks from the Xinglongtai buried hill, Western depression of Liaohe basin, China. *Bulletin* 89 (10), 1319–1346. doi:10.1306/05230503113

Lyu, W. Y., Zeng, L. B., Zhang, B. J., Miao, F. B., Lyu, P., and Dong, S. Q. (2017). Influence of natural fractures on gas accumulation in the Upper Triassic tight gas sandstones in the northwestern Sichuan Basin, China. *Mar. Petroleum Geol.* 83, 60–72. doi:10.1016/j.marpetgeo.2017.03.004

Lyu, W. Y., Zeng, L. B., Zhou, S. B., Du, X. S., Xia, D. L., Liu, G., et al. (2019). Natural fractures in tight-oil sandstones: A case study of the upper triassic yanchang formation in the southwestern ordos basin, China. *Am. Assoc. Pet. Geol. Bull.* 103 (10), 2343–2367. doi:10.1306/0130191608617115

Maerten, L., Maerten, F., and Lejri, M. (2018). Along fault friction and fluid pressure effects on the spatial distribution of fault-related fractures. *J. Struct. Geol.* 108, 198–212. doi:10.1016/j.jsg.2017.10.008

Maréchal, J. C., Dewandel, B., and Subrahmanyam, K. (2004). Use of hydraulic tests at different scales to characterize fracture network properties in the weathered-fractured layer of a hard rock aquifer. *Water Resour. Res.* 40 (11). doi:10.1029/2004WR003137

Nabway, B. S., and Kassab, M. A. (2013). Porosity-reducing and porosity-enhancing diagenetic factors for some carbonate microfacies: A guide for petrophysical facies discrimination. *Arab. J. Geosci.* 17 (11), 4523–4539. doi:10.1007/s12517-013-1083-2

Nelson, R. A., Moldovanyi, E. P., Matcek, C. C., Azpiritxaga, I., and Bueno, E. (2000). Production characteristics of the fractured reservoirs of the La Paz field, Maracaibo basin, Venezuelafield, Maracaibo basin, Venezuela. *Am. Assoc. Pet. Geol. Bull.* 84 (11), 1791–1809. doi:10.1306/8626c393-173b-11d7-8645000102c1865d

Ni, J. L., Guo, Y., Wang, Z. M., Liu, J. L., Lin, Y. X., and Li, Y. (2011). Tectonics and mechanisms of uplift in the central uplift belt of the Huimin depression. *J. Earth Sci.* 22 (3), 299–315. doi:10.1007/s12583-011-0183-8

Ni, J. L., Liu, J. L., Tang, X. L., Yang, H. B., Xia, Z. M., and Guo, Q. J. (2013). The wulian metamorphic core complex: A newly discovered metamorphic core complex along the sulu orogenic belt, eastern China. *J. Earth Sci.* 24 (3), 297–313. doi:10.1007/s12583-013-0330-5

Ortega, O. J., Marrett, R. A., and Laubach, S. E. (2006). A scale-independent approach to fracture intensity and average spacing measurement. *Am. Assoc. Pet. Geol. Bull.* 90 (2), 193–208. doi:10.1306/08250505059

Parnell, J. (2010). Potential of palaeofluid analysis for understanding oil charge history. *Geofluids* 10 (1-2). doi:10.1111/j.1468-8123.2009.00268.x

Peng, J. S., Wei, A. J., Sun, Z., Chen, X. L., and Zhao, D. J. (2018). Sinistral strike slip of the zhangjiakou-penglai fault and its control on hydrocarbon accumulation in the northeast of shaleitian bulge, Bohai Bay Basin, east China. *Petroleum Explor. Dev.* 45 (2), 215–226. doi:10.1016/S1876-3804(18)30025-9

Qi, J. F., Li, X. G., Yu, F. S., and Yu, T. C. (2013). Cenozoic structural deformation and expression of the "tan-Lu fault zone" in the west sag of Liaohe depression, bohaiwan basin province, China. *Sci. China Earth Sci.* 56 (10), 1707–1721. doi:10.1007/s11430-013-4617-2

Salah, M. G., and Alsharhan, A. S. (1998). The precambrian basement: A major reservoir in the rifted basin, gulf of suez. *J. Petroleum Sci. Eng.* 19 (3), 201–222. doi:10.1016/S0920-4105(97)00024-7

Shen, B. T., Topias, S., and Mikael, R. (2015). Modelling fracture propagation in anisotropic rock mass. *Rock Mech. Rock Eng.* 48 (3), 1067–1081. doi:10.1007/s00603-014-0621-x

Song, B., Hu, Y. J., Bian, S. Z., Han, H. D., Cui, X. D., and Zhang, J. (2011). Reservoir characteristics of the crystal basement in the Xinglongtai buried-hill, Liaohe Depression. *Acta Pet. Sin.* 32 (1), 77–82. doi:10.1631/jzus.A1000135

Souque, C., Knipe, R. J., Davies, R. K., Jones, P., Welch, M. J., and Lorenz, J. (2019). Fracture corridors and fault reactivation: Example from the chalk, isle of thanet, kent, england. *J. Struct. Geol.* 122, 11–26. doi:10.1016/j.jsg.2018.12.004

Tan, G., Qiu, H., Yu, T., Liu, S., and Hao, J. (2014). Characteristics and main controlling factors of hydrocarbon accumulation in ordovician yingshan formation in yubei area, tarim basin. *Oil Gas Geol.* 35 (1), 26–32. doi:10.11743/ogg20140104

Tong, K. J., Qi, C., Nie, L. L., and Na, F. (2015). Evaluation of effectiveness of metamorphosed basement buried hill reservoirs. *Oil Gas Geol.* 36 (5). doi:10.11743/ogg20150509

Tong, K. J., Zhao, C. M., Lü, Z., Zhang, Y. C., Zheng, H., Xu, S., et al. (2012). Reservoir evaluation and fracture chracterization of the metamorphic buried hill reservoir in Bohai Bay Basin. *Petroleum Explor. Dev.* 39 (1), 62–69. doi:10.1016/S1876-3804(12)60015-9

Vanderhaeghe, O., Burg, J.-P., and Teyssier, C. (1999). Exhumation of migmatites in two collapsed orogens: Canadian cordillera and French variscides. *Geol. Soc. Lond. Spec. Publ.* 154 (1), 181–204. doi:10.1144/GSL.SP.1999.154.01.08

Wan, G., Tang, L., Zhou, X., Yu, Y., and Chen, X. (2009). Tectonic characteristics of the tanlu fault zone in bodong area of Bohai Sea. *Acta Pet. Sin.* 30 (3), 342–346. doi:10.7623/syxb2009004

Wang, G. Z., Li, S. Z., Li, X. Y., Zhao, W. Z., Zhao, S. J., Suo, Y. H., et al. (2019a). Destruction effect on Meso-Neoproterozoic oil-gas traps derived from Meso-Cenozoic deformation in the North China Craton. *Precambrian Res.* 333, 105427. doi:10.1016/j.precamres.2019.105427

Wang, G. Z., Li, S. Z., Wu, Z. P., Suo, Y. H., Guo, L. L., and Wang, P. C. (2019b). Early Paleogene strike-slip transition of the tan-Lu fault zone across the southeast Bohai Bay Basin: Constraints from fault characteristics in its adjacent basins. *Geol. J.* 54 (2), 835–849. doi:10.1002/gj.3344

Wang, R. Y., Ding, W. L., Zhang, Y. Q., Wang, Z., Wang, X. H., He, J. H., et al. (2016). Analysis of developmental characteristics and dominant factors of fractures in lower cambrian marine shale reservoirs: A case study of niutitang formation in cen'gong block, southern China. *J. Petroleum Sci. Eng.* 138, 31–49. doi:10.1016/j.petrol.2015.12.004

Wang, S., and Li, S. (2014). Migmatite and its geodynamic implications. *Earth Sci. Front.* 21 (01), 21–31. CNKI:SUN:DXQY.0.2014-01-003.

Wang, X. H., Wang, R. Y., Ding, W. L., Yin, S., Sun, Y. X., Zhou, X. H., et al. (2017). Development characteristics and dominant factors of fractures and their significance for shale reservoirs: A case study from Є1b2 in the cen'gong block, southern China. *J. Petroleum Sci. Eng.* 159, 988–999. doi:10.1016/j.petrol.2017.08.007

Wang, X., Zhou, X. H., Xu, G. S., Liu, P. B., and Guan, D. Y. (2015). Characteristics and controlling factors of reservoirs in Penglai 9-1 large-scale oilfield in buried granite hills, Bohai Sea. *Oil Gas Geol.* 36 (2), 262–270. doi:10.11743/ogg20150211

Wang, Y., Zhou, L. Y., Liu, S. F., Li, J. Y., and Yang, T. N. (2018). Post-cratonization deformation processes and tectonic evolution of the North China Craton. *Earth-Science Rev.* 177 (1), 320–365. doi:10.1016/j.earscirev.2017.11.017

Xie, Y. H., Zhang, G. C., Shen, P., Liu, L. F., and Yang, S. B. (2018). Formation conditions and exploration direction of large gas field in Bozhong sag of Bohai Bay Basin. *Acta Pet. Sin.* 39 (11), 1199–1210. doi:10.7623/syxb201811001

Xu, C. G., Du, X. F., Liu, X. J., Xu, W., and Hao, Z. W. (2020). Formation mechanism of high-quality deep buried-hill reservoir of Archaean metamorphic rocks and its significance in petroleum exploration in Bohai Sea area. *Acta Geol. Sin.* 41 (2), 235–247,294. doi:10.19762/j.cnki.dizhixuebao.2021132

Xu, S., Hao, F., Xu, C. G., Zou, H. Y., Zhang, X. T., Zong, Y., et al. (2019). Hydrocarbon migration and accumulation in the northwestern Bozhong subbasin, Bohai Bay Basin, China. *J. Petroleum Sci. Eng.* 172, 477–488. doi:10.1016/j.petrol.2018.09.084

Xue, Y. A., and Li, H. Y. (2018). Large condensate gas field in deep archean metamorphic buried hill in Bohai Sea: Discovery and geological significance. *China Offshore Oil Gas* 30 (3), 1–9. doi:10.11935/j.issn.1673-1506.2018.03.001

Xue, Y. A., Li, H. Y., Xu, P., Liu, Q. C., and Cui, H. Z. (2021). Recognition of oil and gas accumulation of Mesozoic covered buried hills in Bohai sea area and the discovery of BZ 13-2 oilfield 33(1), 13–22. doi:10.11935/j.issn.1673-1506.2021.01.002

Yang, K. J., Qi, J. F., Yu, Y. X., Ping, Y. Q., Gao, Q., and Lv, J. (2016). Differential evolution and reservoir forming conditions of buried hills in Liaodong Bay Area. *Nat. Gas. Geosci.* 27 (6), 1014–1024. doi:10.11764/j.issn.1672-1926.2016.06.1014

Ye, T., Chen, A. Q., Hou, M. C., Niu, C. M., and Wang, Q. B. (2021a). Characteristic of the Bodong segment of the Tanlu Fault Zone, Bohai sea area, eastern China: Implications for hydrocarbon exploration and regional tectonic evolution. *J. Petroleum Sci. Eng.* 201, 108478. doi:10.1016/j.petrol.2021.108478

Ye, T., Chen, A. Q., Niu, C. M., Wang, Q. B., and Guo, L. L. (2020a). Characteristics and vertical zonation of large-scale granitic reservoirs, a case study from Penglai oil field in the Bohai Bay Basin, North China. *Geol. J.* 55 (12), 8109–8121. doi:10.1002/gj.3932

Ye, T., Chen, A. Q., Niu, C. M., Wang, Q. B., and Hou, M. C. (2022). Characteristics, controlling factors and petroleum geologic significance of fractures in the archean crystalline basement rocks: A case study of the south jinzhou oilfield in Liaodong Bay depression, north China. *J. Petroleum Sci. Eng.* 208, 109504. doi:10.1016/j.petrol.2021.109504

Ye, T., Chen, A. Q., Niu, C. M., and Wang, Q. B. (2021b). Structural, petrophysical and lithological characterization of crystalline bedrock buried-hill reservoirs: A case study of the southern jinzhou oilfield in offshore Bohai Bay Basin, north China. *J. Petroleum Sci. Eng.* 196, 107950. doi:10.1016/j.petrol.2020.107950

Ye, T., Niu, C. M., Wang, Q. B., Gao, K. S., Sun, Z., and Chen, A. Q. (2020). Identification of metamorphite lithology in paleo buried hill by composition_structure classification: A case from archean in Bohai Sea. *Lithol. Reserv.* 33, 154–164.

Ye, T., Niu, C. M., and Wei, A. J. (2020b). Characteristics and genetic mechanism of large granitic buried-hill reservoir, a case study from PengLai oil field of Bohai Bay Basin, north China. *J. Petroleum Sci. Eng.* 189, 106988. doi:10.1016/j.petrol.2020.106988

Yin, S., Han, C., Wu, Z. H., and Li, Q. M. (2019). Developmental characteristics, influencing factors and prediction of fractures for a tight gas sandstone in a gentle structural area of the Ordos Basin, China. *J. Nat. Gas Sci. Eng.* 72, 103032. doi:10.1016/j.jngse.2019.103032

Yin, S., and Wu, Z. H. (2020). Geomechanical simulation of low-order fracture of tight sandstone. *Mar. Petroleum Geol.* 117, 104359. doi:10.1016/j.marpetgeo.2020.104359

You, L., Xu, S. L., Mao, X. L., Zhong, J., Jiao, Y. Q., and Xiong, X. F. (2021). Reservoir characteristics and genetic mechanisms of the mesozoic granite buried hills in the deep-water of the qiongdongnan basin, northern south China sea. *Acta Geol. sinica-. Engl. Ed.* 95 (1), 259–267. doi:10.1111/1755-6724.14635

Yu, F. S., and Koyi, H. (2016). Cenozoic tectonic model of the Bohai Bay Basin in China. *Geol. Mag.* 153 (5-6), 866–886. doi:10.1017/S0016756816000492

Yue, X. W., Dai, J. S., and Wang, K. (2014). Influence of rock mechanics parameters on fracture development. *J. Geomechanics* 20 (4), 372–378. doi:10.3969/j.issn.1006-6616.2014.04.005

Zeng, L. B., and Li, X. Y. (2009). Fractures in sandstone reservoirs with ultra-low permeability: A case study of the upper triassic yanchang formation in the ordos basin, China. *Am. Assoc. Pet. Geol. Bull.* 93 (4), 461–477. doi:10.1306/09240808047

Zeng, W. T., Zhang, J. C., Ding, W. L., Zhao, S., Zhang, Y. Q., Liu, Z. J., et al. (2013). Fracture development in Paleozoic shale of Chongqing area (South China). Part one: Fracture characteristics and comparative analysis of main controlling factors. *J. Asian Earth Sci.* 75 (5), 251–266. doi:10.1016/j.jseaes.2013.07.014

Zhang, C., Yang, H. X., Feng, J., and Liu, J. L. (2019). Granitic gneiss domes from the Paleoproterozoic orogen in eastern Liaoning: The typical structural styles in hot orogem. *Acta Petrol. Sin.* 35, 2926–2942. doi:10.18654/000-0569/2019.09.20

Zhang, X. M., Shi, W. Z., Hu, Q. H., Zhai, G. Y., Wang, R., Xu, X., et al. (2020). Developmental characteristics and controlling factors of natural fractures in the lower paleozoic marine shales of the upper Yangtze Platform, southern China. *J. Nat. Gas Sci. Eng.* 76, 103191. doi:10.1016/j.jngse.2020.103191

Zhao, G., Ding, W. L., Sun, Y. X., Wang, X. H., Tina, L., Shi, S. Y., et al. (2020). Fracture development characteristics and controlling factors for reservoirs in the Lower Silurian Longmaxi Formation marine shale of the Sangzhi block, Hunan Province, China. *J. Petroleum Sci. Eng.* 184 (0), 106470. doi:10.1016/j.petrol.2019.106470

Zhao, K. K., Jiang, P. F., Feng, Y. J., Sun, X. D., Cheng, L. X., and Zheng, J. W. (2021). Investigation of the characteristics of hydraulic fracture initiation by using maximum tangential stress criterion. *J. Min. Strata Control Eng.* 3 (2), 023520. doi:10.13532/j.jmsce.cn10-1638/td.20201217.001

Zhao, X., Hu, X., Xiao, K., Jia, Y., and Amp, P. E. (2018). Characteristics and major control factors of natural fractures in carbonate reservoirs of Leikoupo Formation in Pengzhou area, Western Sichuan Basin. *Oil Gas Geol.* 39 (1), 30–39,152. SINOPEC. doi:10.11743/ogg20180104

Zhao, X. Z., Jin, F. M., Wang, Q., and Bai, G. P. (2015). Buried-hill play, jizhong subbasin, Bohai Bay Basin: A review and future propespectivity. *Am. Assoc. Pet. Geol. Bull.* 99 (1), 1–26. doi:10.1306/07171413176

Zheng, H., Zhang, J., and Qi, Y. (2020). Geology and geomechanics of hydraulic fracturing in the Marcellus shale gas play and their potential applications to the Fuling shale gas development. *Energy Geosci.* 1 (1–2), 36–46. doi:10.1016/j.engeos.2020.05.002

Zhou, L. H., Li, S. Z., Liu, J. Z., and Gao, Z. P. (2003). The yanshanian structural style and basin prototypes of the mesozoic Bohai Bay Basin. *Prog. Geophys.* 2003 (4), 692–699. doi:10.1016/S0955-2219(02)00073-0

Zhou, X. H., Xiang, H., Yu, S., Wang, G., and Yao, C. H. (2005). Reservoir characteristics and development controlling factors of JZS Neo-Archean metamorphic buried hill reservoir in Bohai Sea. *Petroleum Explor. Dev.* 32 (6), 17–20. doi:10.3321/j.issn:1000-0747.2005.06.004

Zhu, R. X., Zhang, H. F., Zhu, G., Meng, Q. R., Fan, H. R., Yang, J., et al. (2017). Craton destruction and related resources. *Int. J. Earth Sci.* 106 (7), 2233–2257. doi:10.1007/s00531-016-1441-x

Zou, H. Y., Zhao, C. M., Yin, Z. J., Cai, Y. J., and Teng, C. Y. (2013). Outcrop model of fracture development in neoarchean crystalline buried hill in Bohai Bay Basin. *Nat. Gas. Geosci.* 24 (5), 879–885. CNKI:SUN:TDKX.0.2013-05-002.